

---

# ANCER: Anisotropic Certification via Sample-wise Volume Maximization

---

Francisco Eiras<sup>1,3,\*</sup>   Motasem Alfarra<sup>2,\*</sup>   M. Pawan Kumar<sup>1</sup>   Philip H. S. Torr<sup>1</sup>  
 Puneet K. Dokania<sup>1,3</sup>   Bernard Ghanem<sup>2</sup>   Adel Bibi<sup>1,\*</sup>

<sup>1</sup> University of Oxford, United Kingdom

<sup>2</sup> KAUST, Saudi Arabia

<sup>3</sup> Five AI Limited, United Kingdom

## Abstract

Randomized smoothing has recently emerged as an effective tool that enables certification of deep neural network classifiers at scale. All prior art on randomized smoothing has focused on isotropic  $\ell_p$  certification, which has the advantage of yielding certificates that can be easily compared among isotropic methods via  $\ell_p$ -norm radius. However, isotropic certification limits the region that can be certified around an input to *worst-case* adversaries, *i.e.* it cannot reason about other “close”, potentially large, constant prediction safe regions. To alleviate this issue, (i) we theoretically extend the isotropic randomized smoothing  $\ell_1$  and  $\ell_2$  certificates to their generalized *anisotropic* counterparts following a simplified analysis. Moreover, (ii) we propose evaluation metrics allowing for the comparison of general certificates – a certificate is superior to another if it certifies a *superset* region – with the quantification of each certificate through the volume of the certified region. We introduce ANCER, a practical framework for obtaining anisotropic certificates for a given test set sample via volume maximization. Our empirical results demonstrate that ANCER achieves state-of-the-art  $\ell_1$  and  $\ell_2$  certified accuracy on both CIFAR-10 and ImageNet at multiple radii, while certifying substantially larger regions in terms of volume, thus highlighting the benefits of moving away from isotropic analysis. Code used in our experiments is available [in this repository](#).

## 1 Introduction

The well-studied fact that Deep Neural Networks (DNNs) are vulnerable to additive imperceptible noise perturbations has led to a growing interest in developing robust classifiers [1, 2]. A recent promising approach to achieve state-of-the-art provable robustness (*i.e.* a theoretical bound on the output around every input) at the scale of ImageNet [3] is *randomized smoothing* [4, 5]. Given an input  $x$  and a network  $f$ , randomized smoothing constructs  $g(x) = \mathbb{E}_{\epsilon \sim \mathcal{D}}[f(x + \epsilon)]$  such that  $g(x) = g(x + \delta) \forall \delta \in \mathcal{R}$ , where the certification region  $\mathcal{R}$  is characterized by  $x, f$ , and the smoothing distribution  $\mathcal{D}$ . For instance, Cohen *et al.* [5] showed that if  $\mathcal{D} = \mathcal{N}(0, \sigma^2 I)$ , then  $\mathcal{R}$  is an  $\ell_2$ -ball whose radius is determined by  $x, f$  and  $\sigma$ . Since then, there has been significant progress towards the design of  $\mathcal{D}$  leading to the largest  $\mathcal{R}$  for all inputs  $x$ . The interplay between  $\mathcal{R}$  characterized by  $\ell_1, \ell_2$  and  $\ell_\infty$ -balls, and a notion of optimal distribution  $\mathcal{D}$  has also been previously studied [6].

Despite this progress, current randomized smoothing approaches provide certification regions that are *isotropic* in nature, limiting their capacity to certifying smaller and *worst-case* regions. We provide an intuitive example of this behavior in Figure 1. The isotropic nature of  $\mathcal{R}$  in prior art is

---

\*Authors contributed equally; order of first two authors decided by 3 coin flips. Correspondence to: eiras@robots.ox.ac.uk, motasem.alfarra@kaust.edu.sa, adel.bibi@eng.ox.ac.uk.

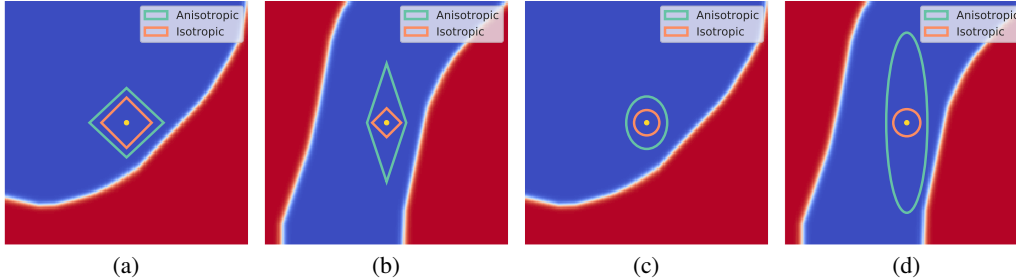


Figure 1: Illustration of the landscape of  $f^y$  (blue corresponds to a higher confidence in  $y$ , the true label) for a region around an input in a toy, 2-dimensional radially separable dataset. For two dataset examples, in (a) and (b) we show the boundaries of the optimal  $\ell_1$  isotropic and anisotropic certificates, while (c) and (d) are the boundaries of the optimal  $\ell_2$  isotropic and anisotropic certificates. A thorough discussion of this figure is presented in Section 3.

due to the common assumption that the smoothing distribution  $\mathcal{D}$  is identically distributed [6–8]. Moreover, comparisons between various randomized smoothing approaches were limited to methods that produce the same  $\ell_p$  certificate, with no clear metrics for comparing with other certificates. In this paper, we address both concerns and present new state-of-the-art certified accuracy results on both CIFAR-10 [9] and ImageNet [3].

Our contributions are threefold. **(i)** We provide a general and simpler analysis compared to prior art [5, 6] that paves the way for the certification of *anisotropic* regions characterized by any norm, holding prior art as special cases. We then specialize our result to regions that, for a positive definite  $\mathbf{A}$ , are ellipsoids, *i.e.*  $\|\mathbf{A}\delta\|_2 \leq c$ , and generalized cross-polytopes, *i.e.*  $\|\mathbf{A}\delta\|_1 \leq c$ , generalizing both  $\ell_2$  [5] and  $\ell_1$  [4, 6] certification (Section 4). **(ii)** We introduce a new evaluation framework to compare methods that certify general (isotropic or anisotropic) regions. We compare two general certificates by defining that a method certifying  $\mathcal{R}_1$  is superior to another certifying  $\mathcal{R}_2$ , if  $\mathcal{R}_1$  is a strict superset to  $\mathcal{R}_2$ . Further, we define a standalone quantitative metric as the volume of the certified region, and specialize it for the cases of ellipsoids and generalized cross-polytopes (Section 5). **(iii)** We propose ANCER, an anisotropic certification method that performs sample-wise (*i.e.* per sample in the test set) region volume maximization (Section 6). We conduct experiments on CIFAR-10 [9] with ResNet18 and WideResNet40, and on ImageNet [3] with ResNet50 (Section 7). In addition to providing anisotropic certificates, we show that restricting ANCER’s certification region to  $\ell_1$  and  $\ell_2$ -balls outperforms state-of-the-art  $\ell_1$  and  $\ell_2$  results from previous works [6, 10]. We also show that the volume of the certified region is significantly larger than all existing methods, thus setting a new state-of-the-art in certified accuracy.

**Notation.** We consider a base classifier  $f : \mathbb{R}^n \rightarrow \mathcal{P}(K)$ , where  $\mathcal{P}(K)$  is a probability simplex over  $K$  classes, *i.e.*  $f^i \geq 0$  and  $\mathbf{1}^\top f = 1$ , for  $i \in \{1, \dots, K\}$ . Further, we use  $(x, y)$  to be a sample input  $x$  and its corresponding true label  $y$  drawn from a test set  $\mathcal{D}_t$ , and  $f^y$  to be the output of  $f$  at the correct class. We use  $\ell_p$  to be the typically defined  $\|\cdot\|_p$  norm ( $p \geq 1$ ), and  $\ell_p^{\mathbf{A}}$  or  $\|\cdot\|_{\mathbf{A},p}$  for  $p = \{1, 2\}$  to be a composite norm defined with respect to a positive definite matrix  $\mathbf{A}$  and a vector  $v$  as  $\|\mathbf{A}^{-1/p}v\|_p$ .

## 2 Related Work

**Verified Defenses.** Since the discovery that DNNs are vulnerable against input perturbations [1, 2], a range of methods have been proposed to build classifiers that are verifiably robust [11]. Techniques in this category include methods ranging from interval bound propagation [12] to semi-definite programming based verification [13] or convex relaxation approaches [14–16]. Despite this progress, these methods do not scale to the networks the community is interested in certifying [17, 18].

**Randomized Smoothing.** The first works on randomized smoothing used Laplacian [4, 19] and Gaussian [5] distributions to obtain  $\ell_1$  and  $\ell_2$ -ball certificates, respectively. Several subsequent works improved the performance of smooth classifiers by training the base classifier using adversarial augmentation [20], regularization [21], or general adjustments to training routines [22]. Previous work extended [5, 19, 23] to a variety of other isotropic smoothing distributions, yielding other



Figure 2: Visualization of a CIFAR-10 image  $x$  and an example  $x + \delta$  of an imperceptible change that *is not* inside the optimal isotropic certified region, but *is* covered by the anisotropic certificate.

$\ell_p$ -norm certificates [6, 24, 25]. Concurrently, Dvijotham *et al.* [26] developed a framework to handle arbitrary smoothing measures in any  $\ell_p$ -norm; however, the certification process requires significant hyperparameter tuning. This was followed by a complementary data-dependent smoothing approach, where the parameters of the smoothing distribution were optimized per test set *sample* to maximize the certified radius at an individual input [10]. All prior works considered smoothing with *isotropic* distributions and hence certified isotropic  $\ell_p$ -ball regions. In this paper, we extend randomized smoothing to certify *anisotropic* regions, by pairing it with a generalization of the data-dependent framework from [10] so as to maximize the certified region at each input point.

### 3 Motivating Anisotropic Certificates

Certification approaches aim to find the *safe* region  $\mathcal{R}$ , where  $\arg \max_i f^i(x) = \arg \max_i f^i(x + \delta) \forall \delta \in \mathcal{R}$ . Recent randomized smoothing techniques perform this certification by explicitly optimizing the isotropic  $\ell_p$  certified region around each input [10], obtaining state-of-the-art performance as a result. Despite this  $\ell_p$  optimality, we note that any  $\ell_p$ -norm certificate is *worst-case* from the perspective of that norm, as it avoids adversary regions by limiting its certificate to the  $\ell_p$ -closest adversary. This means that it can only enjoy a radius that is at most equal to the distance to the closest decision boundary. However, decision boundaries of general classifiers are complex, non-linear, and non-radially distributed with respect to a generic input sample [27]. This is evidenced by the fact that, within a reasonably small  $\ell_p$ -ball around an input, there are often only a small set of adversary directions [28, 29] (*e.g.* see the decision boundaries in Figure 1). As such, while  $\ell_p$ -norm certificates are useful to reason about worst-case performance and are simple to obtain given previous works [5, 6, 23], they are otherwise uninformative in terms of the shape of decision boundaries, *i.e.* which regions around the input are safe.

To visualize these concepts, we illustrate the decision boundaries of a base classifier  $f$  trained on a toy 2-dimensional, radially separable (with respect to the origin) binary classification dataset, and consider two different input test samples (see Figure 1). We compare the *optimal* isotropic and anisotropic certified regions of different shapes at these points. In Figures 1a and 1b, we compare an isotropic cross-polytope (of the form  $\|\delta\|_1 \leq r$ ) with an anisotropic generalized cross-polytope (of the form  $\|\mathbf{A}\delta\|_1 \leq r$ ), while in Figures 1c and 1d we compare an isotropic  $\ell_2$  ball (of the form  $\|\delta\|_2 \leq r$ ) with an anisotropic ellipsoid (of the form  $\|\mathbf{A}\delta\|_2 \leq r$ ). Notice that in Figures 1a and 1c, due to the curvature of the classification boundary (shown in white), the optimal certification region is isotropic in nature, which is evidenced by the similarities of the optimal isotropic and anisotropic certificates. On the other hand, in Figures 1b and 1d, the location of the decision boundary allows for the anisotropic certified regions to be considerably larger than their isotropic counterparts, as they are not as constrained by the closest decision boundary, *i.e.* the *worst-case* performance. We note that these differences are further highlighted in higher dimensions, and we study them for a single CIFAR-10 test set sample in Appendix A.

As observed from the previous examples, anisotropic certification reasons more closely about the shape of the decision boundaries, allowing for further insights into constant prediction (safe) directions. In Figure 2, we present a series of test set images  $x$ , as well as practically indistinguishable  $x + \delta$  images which *are not inside* the optimal certified isotropic  $\ell_2$ -balls for each input sample, yet *are within* the anisotropic certified regions. This showcases the merits of using anisotropic certification for characterizing larger safe regions.

## 4 Anisotropic Certification

One of the main obstacles in enabling anisotropic certification is the complexity of the analysis required. To alleviate this, we follow a Lipschitz argument first observed in [20] and propose a simple and general certification analysis in Section 4.1. Further, we show two specializations for anisotropic certification, namely ellipsoids (Section 4.2) and generalized cross-polytopes (Section 4.3). Our analysis complements approaches in earlier randomized smoothing works, which were based on Neyman-Pearson’s lemma [5] or the Level-Set and Differential Method [6]. All proofs in this section can be found in Appendix B.

### 4.1 Theoretical Foundation

**Proposition 1.** *Consider a differentiable function  $g : \mathbb{R}^n \rightarrow \mathbb{R}$ . If  $\sup_x \|\nabla g(x)\|_* \leq L$  where  $\|\cdot\|_*$  has a dual norm  $\|z\| = \max_x z^\top x$  s.t.  $\|x\|_* \leq 1$ , then  $g$  is  $L$ -Lipschitz under norm  $\|\cdot\|_*$ , that is  $|g(x) - g(y)| \leq L\|x - y\|$ .*

Given the previous proposition, we formalize  $\|\cdot\|$  certification as follows:

**Theorem 1.** *Let  $g : \mathbb{R}^n \rightarrow \mathbb{R}^K$ ,  $g^i$  be  $L$ -Lipschitz continuous under norm  $\|\cdot\|_* \forall i \in \{1, \dots, K\}$ , and  $c_A = \arg \max_i g^i(x)$ . Then, we have  $\arg \max_i g^i(x + \delta) = c_A$  for all  $\delta$  satisfying:*

$$\|\delta\| \leq \frac{1}{2L} \left( g^{c_A}(x) - \max_c g^{c \neq c_A}(x) \right).$$

Theorem 1 provides an  $\|\cdot\|$  norm robustness certificate for any  $L$ -Lipschitz classifier  $g$  under  $\|\cdot\|_*$ . The certificate is only informative when one can attain a tight *non-trivial* estimate of  $L$ , ideally  $\sup_x \|\nabla g(x)\|_*$ , which is generally difficult when  $g$  is an arbitrary neural network. In light of Theorem 1, randomized smoothing can be viewed **differently** as an instance of Theorem 1 with the favorable property that the constructed smooth classifier  $g$  enjoys an analytical form for  $L = \sup_x \|\nabla g(x)\|_*$  by design. Following the view of Theorem 1 in the randomized smoothing setting and to obtain an informative  $\|\cdot\|$  certificate, one must, for an arbitrary choice of a smoothing distribution, compute the analytic Lipschitz constant  $L$  under  $\|\cdot\|_*$  for the smooth  $g$ . While there can exist a notion of “optimal” smoothing distribution for a given choice of  $\|\cdot\|$  certificate, as in part addressed earlier for the isotropic  $\ell_1$ ,  $\ell_2$  and  $\ell_\infty$  certificates [6], this is not the focus of this paper. The choice of the smoothing distribution in later sections is merely inspired by previous work for the sole purpose of granting anisotropic certificates.

In Sections 4.2 and 4.3, we will use the recipe laid down earlier for Theorem 1 in the randomized smoothing setting to obtain certificates for anisotropic regions<sup>2</sup>.

### 4.2 Certifying Ellipsoids

In this section, we consider the certification under  $\ell_2^\Sigma$  norm, or  $\|\delta\|_{\Sigma,2} = \sqrt{\delta^\top \Sigma^{-1} \delta}$ , that has a dual norm  $\|\delta\|_{\Sigma^{-1},2}$ . Note that both  $\|\delta\|_{\Sigma,2} \leq r$  and  $\|\delta\|_{\Sigma^{-1},2} \leq r$  define an ellipsoid. Despite that the following results hold for any positive definite  $\Sigma$ , we assume for efficiency reasons that  $\Sigma$  is diagonal throughout. First, we consider the anisotropic Gaussian smoothing distribution  $\mathcal{N}(0, \Sigma)$  with the smooth classifier defined as  $g_\Sigma(x) = \mathbb{E}_{\epsilon \sim \mathcal{N}(0, \Sigma)} [f(x + \epsilon)]$ . Considering the classifier  $\Phi^{-1}(g_\Sigma(x))$ , where  $\Phi$  is the standard Gaussian CDF, and following Theorem 1 to grant an  $\ell_2^\Sigma$  certificate for  $\Phi^{-1}(g_\Sigma(x))$ , we derive the Lipschitz constant  $L$  under  $\|\cdot\|_{\Sigma^{-1},2}$ , in the following proposition.

**Proposition 2.**  $\Phi^{-1}(g_\Sigma(x))$  is 1-Lipschitz (i.e.  $L = 1$ ) under the  $\|\cdot\|_{\Sigma^{-1},2}$  norm.

Since  $\Phi^{-1}$  is a strictly increasing function, by combining Proposition 2 with Theorem 1, we have:

**Corollary 1.** *Let  $c_A = \arg \max_i g_\Sigma^i(x)$ , then  $\arg \max_i g_\Sigma^i(x + \delta) = c_A$  for all  $\delta$  satisfying:*

$$\|\delta\|_{\Sigma,2} \leq \frac{1}{2} \left( \Phi^{-1}(g_\Sigma^{c_A}(x)) - \Phi^{-1}\left(\max_c g_\Sigma^{c \neq c_A}(x)\right) \right).$$

Corollary 1 holds the  $\ell_2$  certification from previous works a special case where  $\Sigma = \sigma^2 I$  [5, 21].<sup>3</sup>

<sup>2</sup>Our analysis also grants a certificate for a mixture of Gaussians smoothing distribution (see Appendix B.1).

<sup>3</sup>A similar result was derived in the appendix of [30, 31] with a more involved analysis by extending Neyman-Pearson’s lemma.

### 4.3 Certifying Generalized Cross-Polytopes

Here we consider certification under the  $\ell_1^\Lambda$  norm defining a generalized cross-polytope, *i.e.* the set  $\{\delta : \|\delta\|_{\Lambda,1} = \|\Lambda^{-1}\delta\|_1 \leq r\}$ , as opposed to the  $\ell_1$ -bounded set that defines a cross-polytope, *i.e.*  $\{\delta : \|\delta\|_1 \leq r\}$ . As with the ellipsoid case and despite that the following results hold for any positive definite  $\Lambda$ , for the sake of efficiency, we assume  $\Lambda$  to be diagonal throughout. For generalized cross-polytope certification, we consider an anisotropic Uniform smoothing distribution  $\mathcal{U}$ , which defines the smooth classifier  $g_\Lambda(x) = \mathbb{E}_{\epsilon \sim \mathcal{U}_{[-1,1]^n}} [f(x + \Lambda\epsilon)]$ . Following Theorem 1 and to certify under the  $\ell_1^\Lambda$  norm, we compute the Lipschitz constant of  $g_\Lambda$  under the  $\|\Lambda x\|_\infty$  norm, which is the dual norm of  $\|\cdot\|_{\Lambda,1}$  (see Appendix B), in the next proposition.

**Proposition 3.** *The classifier  $g_\Lambda$  is  $1/2$ -Lipschitz (*i.e.*  $L = 1/2$ ) under the  $\|\Lambda x\|_\infty$  norm.*

Similar to Corollary 1, by combining Proposition 3 with Theorem 1, we have that:

**Corollary 2.** *Let  $c_A = \arg \max_i g_\Lambda^i(x)$ , then  $\arg \max_i g_\Lambda^i(x + \delta) = c_A$  for all  $\delta$  satisfying:*

$$\|\delta\|_{\Lambda,1} = \|\Lambda^{-1}\delta\|_1 \leq \left( g_\Lambda^{c_A}(x) - \max_c g_\Lambda^{c \neq c_A}(x) \right).$$

Corollary 2 holds the  $\ell_1$  certification of from previous works under the special case  $\Lambda = \lambda I$  [4, 6].

## 5 Evaluating Anisotropic Certificates

With the anisotropic certification framework presented in the previous section, the question arises: ‘‘Given two general (isotropic or anisotropic) certification regions  $\mathcal{R}_1$  and  $\mathcal{R}_2$ , how can one effectively compare them?’’. We propose the following definition to address this issue.

**Definition 1.** *For a given input point  $x$ , consider the two certification regions  $\mathcal{R}_1$  and  $\mathcal{R}_2$  obtained for two classifiers  $f_1$  and  $f_2$ , *i.e.*  $\mathcal{A}_1 = \{\delta : \arg \max_c f_1^c(x) = \arg \max_c f_1^c(x + \delta), \forall \delta \in \mathcal{R}_1\}$  and  $\mathcal{A}_2 = \{\delta : \arg \max_c f_2^c(x) = \arg \max_c f_2^c(x + \delta), \forall \delta \in \mathcal{R}_2\}$  where  $\arg \max_c f_1^c(x) = \arg \max_c f_2^c(x)$ . We say  $\mathcal{A}_1$  is a ‘‘superior certificate’’ to  $\mathcal{A}_2$  (*i.e.*  $\mathcal{A}_1 \succ \mathcal{A}_2$ ), if and only if,  $\mathcal{A}_1 \supset \mathcal{A}_2$ .*

This definition is a natural extension from the radius-based comparison of  $\ell_p$ -ball certificates, providing a basis for evaluating anisotropic certification. To compare an anisotropic to an isotropic region of certification, it is not immediately clear how to (i) check that an anisotropic region is a superset to the isotropic region, and (ii) if it were a superset, how to quantify the improvement of the anisotropic region over the isotropic counterpart. In Sections 5.1 and 5.2, we tackle these issues for the particular cases of ellipsoid and generalized cross-polytope certificates.

### 5.1 Evaluating Ellipsoid Certificates

**Comparing  $\ell_2$ -Balls to  $\ell_2^\Sigma$ -Ellipsoids (Specialization of Definition 1).** Recall that if  $\Sigma = \sigma^2 I$ , our ellipsoid certification in Corollary 1 recovers as a special case the isotropic  $\ell_2$ -ball certification from [5, 20, 21]. Consider the certified regions  $\mathcal{R}_1 = \{\delta : \|\delta\|_2 \leq \tilde{\sigma} r_1\}$  and  $\mathcal{R}_2 = \{\delta : \|\delta\|_{\Sigma,2} = \sqrt{\delta^\top \Sigma^{-1} \delta} \leq r_2\}$  for given  $r_1, r_2 > 0$ . Since we take  $\Sigma = \text{diag}\{\sigma_i^2\}_{i=1}^n$ , the maximum enclosed  $\ell_2$ -ball for the ellipsoid  $\mathcal{R}_2$  is given by the set  $\mathcal{R}_3 = \{\delta : \|\delta\|_2 \leq \min_i \sigma_i r_2\}$ , and thus  $\mathcal{R}_2 \supseteq \mathcal{R}_3$ . Therefore, it suffices that  $\mathcal{R}_3 \supseteq \mathcal{R}_1$  (*i.e.*  $\min_i \sigma_i r_2 \geq \tilde{\sigma} r_1$ ), to say that  $\mathcal{R}_2$  is a superior certificate to the isotropic  $\mathcal{R}_1$  as per Definition 1.

**Quantifying  $\ell_2^\Sigma$  Certificates.** The aforementioned specialization is only concerned with whether our ellipsoid certified region  $\mathcal{R}_2$  is ‘‘superior’’ to the isotropic  $\ell_2$ -ball without quantifying it. A natural solution is to directly compare the volumes of the certified regions. Since the volume of an ellipsoid given by  $\mathcal{R}_2$  is  $\mathcal{V}(\mathcal{R}_2) = r_2^n \sqrt{\pi^n} / \Gamma(n/2 + 1) \prod_{i=1}^n \sigma_i$  [32], we directly compare the *proxy radius*  $\tilde{R}$  defined for  $\mathcal{R}_2$  as  $\tilde{R} = r_2 \sqrt[n]{\prod_i \sigma_i}$ , since larger  $\tilde{R}$  correspond to certified regions with larger volumes. Note that  $\tilde{R}$ , which is the  $n^{\text{th}}$  root of the volume up to a constant factor, can be seen as a generalization to the certified radius in the case when  $\sigma_i = \sigma \forall i$ .

### 5.2 Evaluating Generalized Cross-Polytope Certificates

**Comparing  $\ell_1$ -Balls to  $\ell_1^\Lambda$ -Generalized Cross-Polytopes (Specialization of Definition 1).** Consider the certificates  $\mathcal{S}_1 = \{\delta : \|\delta\|_1 \leq \tilde{\lambda} r_1\}$ ,  $\mathcal{S}_2 = \{\delta : \|\delta\|_{\Lambda,1} = \|\Lambda^{-1}\delta\|_1 \leq r_2\}$ , and



$\mathcal{S}_3 = \{\delta : \|\delta\|_1 \leq \min_i \lambda_i r_2\}$ , where we take  $\Lambda = \text{diag}(\{\lambda_i\}_{i=1}^n)$ . Note that since  $\mathcal{S}_2 \supseteq \mathcal{S}_3$ , then as per Definition 1, it suffices that  $\mathcal{S}_3 \supseteq \mathcal{S}_1$  (i.e.  $\min_i \lambda_i r_2 \geq \lambda r_1$ ) to say that the anisotropic generalized cross-polytope  $\mathcal{S}_2$  is superior to the isotropic  $\ell_1$ -ball  $\mathcal{S}_1$ .

**Quantifying  $\ell_1^\Lambda$  Certificates.** Following the approach proposed in the  $\ell_2^\Sigma$  case, we quantitatively compare the generalized cross-polytope certification of Corollary 2 to the  $\ell_1$  certificate through the volumes of the two regions. We first present the volume of the generalized cross-polytope.

**Proposition 4.**  $\mathcal{V}(\{\delta : \|\Lambda^{-1}\delta\|_1 \leq r\}) = \frac{(2r)^n}{n!} \prod_i \lambda_i$ .

Following this definition, we define the *proxy radius* for  $\mathcal{S}_2$  in this case to be  $\tilde{R} = r_2 \sqrt[n]{\prod_{i=1}^n \lambda_i}$ . As with the  $\ell_2$  case, larger  $\tilde{R}$  correspond certified regions with larger volumes. As in the ellipsoid case,  $\tilde{R}$  can be seen as a generalization to the certified radius when  $\lambda_i = \lambda \forall i$ .

## 6 ANCER: Sample-wise Volume Maximization for Anisotropic Certification

Given the results from the previous sections, we are now equipped to certify anisotropic regions, in particular ellipsoids and generalized cross-polytopes. As mentioned in Section 4, these regions are generally defined as  $\mathcal{R} = \{\delta : \|\delta\|_{\Theta,p} \leq r^p\}$  for a given parameter of the smoothing distribution  $\Theta = \text{diag}(\{\theta_i\}_{i=1}^n)$ , an  $\ell_p$ -norm ( $p \in \{1, 2\}$ ), and a gap value of  $r^p \in \mathbb{R}^+$ . At this point, one could simply take an anisotropic distribution with arbitrarily chosen parameters  $\Theta$  and certify a trained network at any input point  $x$ , in the style of what was done in the previous randomized smoothing literature with isotropic distributions [5, 20, 21]. However, the choice of  $\Theta$  is more complex in the anisotropic case. A fixed choice of anisotropic  $\Theta$  could severely underperform the isotropic case – take, for example, the anisotropic distribution of Figure 1d applied to the input of Figure 1c.

Instead of taking a fixed  $\Theta$ , we generalize the framework introduced in [10], where parameters of the smoothing distribution are optimized per input test point (i.e. in a *sample-wise* fashion) so as to maximize the resulting certificate. The goal of the optimization in [10] is, at a point  $x$ , to maximize the isotropic  $\ell_2$  region described in Section 4.2 (i.e.  $\{\delta : \|\delta\|_2 \leq \sigma^x r^p(x, \sigma^x)\}$ ), where  $r^p$  is the gap and a function of  $x$  and  $\sigma^x \in \mathbb{R}^+$ . In the isotropic  $\ell_p$  case, this generalizes to maximizing the region  $\{\delta : \|\delta\|_p \leq \theta^x r^p(x, \theta^x)\}$ , which can be achieved by maximizing radius  $\theta^x r^p(x, \theta^x)$  through  $\theta^x \in \mathbb{R}^+$ , obtaining  $r_{\text{iso}}^*$  [10].

For the general anisotropic case, we propose ANCER, whose objective is to maximize the volume of the certified region through the *proxy radius*, while satisfying the *superset* condition with respect to the maximum isotropic  $\ell_2$  radius,  $r_{\text{iso}}^*$ . In the case of the ellipsoids and generalized cross-polytopes as presented in Sections 5.1 and 5.2, respectively, ANCER’s optimization problem can be written as:

$$\arg \max_{\Theta^x} r^p(x, \Theta^x) \sqrt[n]{\prod_i \theta_i^x} \quad \text{s.t.} \quad \min_i \theta_i^x r^p(x, \Theta^x) \geq r_{\text{iso}}^* \quad (1)$$

where  $r^p(x, \Theta^x)$  is the gap value under the anisotropic smoothing distribution. We iteratively solve a relaxed version of Equation (1) using Adam [33], with further details presented in Appendix C.

## 7 Experiments

We now study the empirical performance of ANCER to obtain  $\ell_2^\Sigma$ ,  $\ell_1^\Lambda$ ,  $\ell_2$  and  $\ell_1$  certificates on networks trained using randomized smoothing methods found in the literature. In this section, we show that ANCER is able to achieve (i) improved performance on those networks in terms of  $\ell_2$  and  $\ell_1$  certification when compared to certification baselines that smooth using a fixed isotropic  $\sigma$  (Fixed  $\sigma$ ) [5, 6, 20, 21] or a data-dependent isotropic one (Isotropic DD) [10]; and (ii) a significant improvement in terms of the  $\ell_2^\Sigma$  and  $\ell_1^\Lambda$ -norm certified region obtained by the same methods – compared by computing the *proxy radius* of the certified regions – thus generally satisfying the conditions of a superior certificate proposed in Definition 1.

We follow an evaluation procedure as similar as possible to the ones described in [5, 6, 10, 20, 21] by using code and pre-trained networks whenever available and by performing experiments on CIFAR-10 [9] and ImageNet [3], certifying the entire CIFAR-10 test set and a subset of 500 examples from

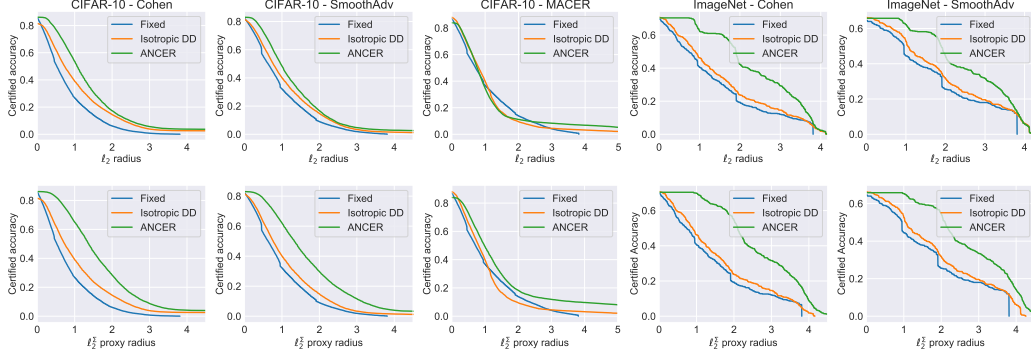


Figure 3: Distribution of top-1 certified accuracy as a function of  $\ell_2$  radius (top) and  $\ell_2^\Sigma$ -norm proxy radius (bottom) obtained by different certification methods on CIFAR-10 and ImageNet.

the ImageNet test set. For the implementation of ANCER, we solve Equation (1) with Adam [33] for 100 iterations, where the certification gap  $r^p(x, \Theta^x)$  is estimated at each iteration using 100 noise samples per test point (see Appendix C) and  $\Theta^x$  in Equation (1) is initialized with the Isotropic DD solution from [10]. Further details of the experimental setup can be found in Appendix D.

As in previous works,  $\ell_p$  **certified accuracy** at radius  $R$  is defined as the portion of the test set  $\mathcal{D}_t$  for which the smooth classifier correctly classifies with an  $\ell_p$  certification radius of at least  $R$ . In a similar fashion, we define the anisotropic  $\ell_2^\Sigma/\ell_1^\Lambda$  certified accuracy at a proxy radius of  $\tilde{R}$  (as defined in Section 5) to be the portion of  $\mathcal{D}_t$  in which the smooth classifier classifies correctly with an  $\ell_2^\Sigma/\ell_1^\Lambda$ -norm certificate of an  $n^{\text{th}}$  root volume of at least  $\tilde{R}$ . We also report **average certified radius** ( $ACR$ ) defined as  $\mathbb{E}_{x,y \sim \mathcal{D}_t}[R_x \mathbb{1}(g(x) = y)]$  [10, 21] as well as **average certified proxy radius** ( $AC\tilde{R}$ ) defined as  $\mathbb{E}_{x,y \sim \mathcal{D}_t}[\tilde{R}_x \mathbb{1}(g(x) = y)]$ , where  $R_x$  and  $\tilde{R}_x$  denote the radius and proxy radius at  $x$  with a true label  $y$  for a smooth classifier  $g$ . Recall that in the isotropic case, the proxy radius is, by definition, the same as the radius for a given  $\ell_p$ -norm. For each classifier, we ran experiments on the  $\sigma$  values reported in the original work (with the exception of [6], see Section 7.2). For the sake of brevity, we report in this section the top-1 certified accuracy plots,  $ACR$  and  $AC\tilde{R}$  per radius across  $\sigma$ , as in [20, 21, 10]. The performance of each method per  $\sigma$  is presented in Appendix F.

### 7.1 Ellipsoid certification ( $\ell_2$ and $\ell_2^\Sigma$ -norm certificates)

We perform the comparison of  $\ell_2$ -ball vs.  $\ell_2^\Sigma$ -ellipsoid certificates via Gaussian smoothing using networks trained following the procedures defined in COHEN [5], SMOOTHADV [20], and MACER [21]. For each of these, we report results on ResNet18 trained using  $\sigma \in \{0.12, 0.25, 0.5, 1.0\}$  for CIFAR-10, and ResNet50 using  $\sigma \in \{0.25, 0.5, 1.0\}$  for ImageNet. For details of the training procedures, see Appendix D.1. Figure 3 plots top-1 certified accuracy as a function of the  $\ell_2$  radius (top) and of the  $\ell_2^\Sigma$ -norm proxy radius (bottom) per trained network and dataset, while Table 1 presents an overview of the certified accuracy at various  $\ell_2$  radii, as well as  $\ell_2$   $ACR$  and  $\ell_2^\Sigma$ -norm  $AC\tilde{R}$ . Recall that, following the considerations in Section 5.1, the  $\ell_2$  certificate obtained through ANCER is the maximum enclosed isotropic  $\ell_2$ -ball in the  $\ell_2^\Sigma$  ellipsoid.

First, we note that sample-wise certification (Isotropic DD and ANCER) achieves higher certified accuracy than fixed  $\sigma$  across the board. This mirrors the findings in [10], since certifying with a fixed  $\sigma$  for all samples struggles with the robustness/accuracy trade-off first mentioned in [5], whereas the data-dependent solutions explicitly optimize  $\sigma$  per sample to avoid it. More importantly, ANCER achieves new state-of-the-art  $\ell_2$  certified accuracy at most radii in Table 1, e.g. at radius 0.5 ANCER brings certified accuracy to 77% (from 66%) and 70% (from 62%) on CIFAR-10 and ImageNet, respectively, yielding relative percentage improvements in  $ACR$  between 13% and 47% when compared to Isotropic DD. While the results are significant, it might not be immediately clear why maximizing the volume of an ellipsoid with ANCER results in a larger maximum enclosed  $\ell_2$ -ball certificate in  $\ell_2^\Sigma$  ellipsoid when compared to optimizing the  $\ell_2$ -ball with Isotropic DD. We explore this phenomenon in Section 7.3.

As expected,  $\ell_2^\Sigma$   $AC\tilde{R}$  is substantially improved using ANCER in all cases – with relative improvements in  $AC\tilde{R}$  between 38% and 63%. The joint results, certification with  $\ell_2$  and  $\ell_2^\Sigma$ , establish that

Table 1: Comparison of top-1 certified accuracy at different  $\ell_2$  radii,  $\ell_2$  average certified radius ( $ACR$ ) and  $\ell_2^\Sigma$  average certified proxy radius ( $AC\tilde{R}$ ) obtained by using the isotropic  $\sigma$  used for training the networks (Fixed  $\sigma$ ); the isotropic data-dependent (Isotropic DD) optimization scheme from [10]; and ANCER’s data-dependent anisotropic optimization.

CIFAR-10	Certification	Accuracy @ $\ell_2$ radius (%)							$\ell_2 ACR$	$\ell_2^\Sigma AC\tilde{R}$
		0.0	0.25	0.5	1.0	1.5	2.0	2.5		
COHEN [5]	Fixed $\sigma$	86	71	51	27	14	6	2	0.722	0.722
	Isotropic DD	82	76	62	39	24	14	8	1.117	1.117
	ANCER	86	85	77	53	31	17	10	<b>1.449</b>	<b>1.825</b>
SMOOTHADV [20]	Fixed $\sigma$	82	72	55	32	19	9	5	0.834	0.834
	Isotropic DD	82	75	63	40	25	15	7	1.011	1.011
	ANCER	83	81	73	48	30	17	8	<b>1.224</b>	<b>1.641</b>
MACER [21]	Fixed $\sigma$	87	76	59	37	24	14	9	0.970	0.970
	Isotropic DD	88	80	66	40	17	9	6	1.007	1.007
	ANCER	84	80	67	34	15	11	9	<b>1.136</b>	<b>1.514</b>

ImageNet	Certification	Accuracy @ $\ell_2$ radius (%)							$\ell_2 ACR$	$\ell_2^\Sigma AC\tilde{R}$
		0.0	0.5	1.0	1.5	2.0	2.5	3.0		
COHEN [5]	Fixed $\sigma$	70	56	41	31	19	14	12	1.098	1.098
	Isotropic DD	71	59	46	36	24	19	15	1.234	1.234
	ANCER	70	70	62	61	42	36	29	<b>1.810</b>	<b>1.981</b>
SMOOTHADV [20]	Fixed $\sigma$	65	59	44	38	26	20	18	1.287	1.287
	Isotropic DD	66	62	53	41	32	24	20	1.428	1.428
	ANCER	66	66	62	58	44	37	32	<b>1.807</b>	<b>1.965</b>

ANCER certifies the  $\ell_2$ -ball region obtained by previous approaches, in addition to a much larger region captured by the  $\ell_2^\Sigma$  certified accuracy and  $AC\tilde{R}$ , and therefore is, according to Definition 1, generally superior to the Isotropic DD one.

## 7.2 Generalized Cross-Polytope certification ( $\ell_1$ and $\ell_1^\Lambda$ -norm certificates)

To investigate  $\ell_1$ -ball vs.  $\ell_1^\Lambda$ -generalized cross-polytope certification via Uniform smoothing, we compare ANCER to the  $\ell_1$  state-of-the-art results from RS4A [6]. While the authors of the original work report best certified accuracy based on 15 networks trained at different  $\sigma$  levels between 0.15 and 3.5 on CIFAR-10 (WideResNet40) and ImageNet (ResNet50) and due to limited computational resources, we perform the analysis on a subset of those networks with  $\sigma = \{0.25, 0.5, 1.0\}$ . We reproduce the results in [6] as closely as possible, with details of the training procedure presented in Appendix D.2. Figure 4 shows the top-1 certified accuracy as a function of the  $\ell_1$  radius (top) and of the  $\ell_1^\Lambda$ -norm proxy radius (bottom) for RS4A, and Table 2 shows an overview  $ACR$  at various  $\ell_1$  radii, as well as  $\ell_1 ACR$  and  $\ell_1^\Lambda AC\tilde{R}$ .

As with the ellipsoid case, we notice that ANCER outperforms both Fixed  $\sigma$  and Isotropic DD for most  $\ell_1$  radii, establishing new state-of-the-art results in CIFAR-10 at radii 0.5 and 1.0, and ImageNet at radii 0.5 (compared to previous results reported in [6]). Once more and as expected, ANCER significantly improves the  $\ell_1^\Lambda AC\tilde{R}$  for all radii, pointing to substantially larger certificates than the isotropic case. These results also establish that ANCER certifies the  $\ell_1$ -ball region obtained by previous work, in addition to the larger region defined by the  $\ell_1^\Lambda$  certificate, and thus we can consider it generally superior (with respect to Definition 1) to Isotropic DD.

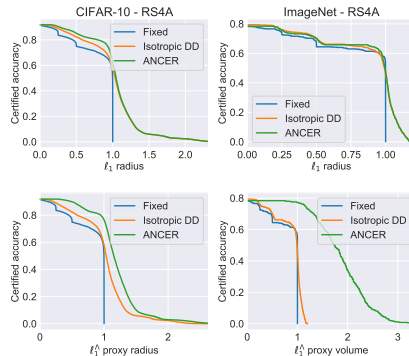


Figure 4: Distribution of top-1 certified accuracy as a function of  $\ell_1$  radius (top) and  $\ell_1^\Lambda$ -norm proxy radius (bottom) obtained by different certification methods on CIFAR-10 and ImageNet.



Table 2: Comparison of top-1 certified accuracy at different  $\ell_1$  radii,  $\ell_1$  average certified radius ( $ACR$ ) and  $\ell_1^\Delta$  average certified proxy radius ( $AC\tilde{R}$ ) obtained by using the isotropic  $\sigma$  used for training the networks (Fixed  $\sigma$ ); the isotropic data-dependent (Isotropic DD) optimization scheme from [10]; and ANCER’s data-dependent anisotropic optimization.

CIFAR-10	Certification	Accuracy @ $\ell_1$ radius (%)							$\ell_1 ACR$	$\ell_1^\Delta AC\tilde{R}$
		0.0	0.25	0.5	0.75	1.0	1.5	2.0		
RS4A [6]	Fixed $\sigma$	92	83	75	71	46	0	0	0.775	0.775
	Isotropic DD	92	89	82	76	58	6	2	0.946	0.946
	ANCER	92	90	84	80	63	6	2	<b>0.980</b>	<b>1.104</b>
<b>ImageNet</b>										
RS4A [6]	Fixed $\sigma$	78	73	67	63	0	0	0	0.683	0.683
	Isotropic DD	79	76	70	65	46	0	0	0.729	0.729
	ANCER	78	76	70	66	48	0	0	<b>0.730</b>	<b>1.513</b>

### 7.3 Why does ANCER improve upon Isotropic DD’s $\ell_p$ certificates?

As observed in Sections 7.1 and 7.2, ANCER’s  $\ell_2$  and  $\ell_1$  certificates outperform the the corresponding certificates obtained by Isotropic DD. To explain this, we compare the  $\ell_2$  certified region obtained by ANCER, defined in Section 6 as  $\{\delta : \|\delta\|_2 \leq \min_i \sigma_i^x r(x, \Sigma^x)\}$ , to the one by Isotropic DD defined as  $\{\delta : \|\delta\|_2 \leq \sigma^x r(x, \sigma^x)\}$ . We observe that the radius of both of these certificates can be separated into a  $\sigma$ -factor ( $\sigma^x$  vs.  $\sigma_{\min}^x = \min_i \sigma_i^x$ ) and a *gap*-factor ( $r(x, \sigma^x)$  vs.  $r(x, \Sigma^x)$ ). We posit the seemingly surprising result can be attributed to the computation of the gap-factor  $r$  using an anisotropic, optimized distribution. However, another potential explanation would be that ANCER benefits from a prematurely stopped initialization provided by Isotropic DD, thus achieving a better  $\sigma_{\min}^x$  than the isotropic  $\sigma^x$  when given further optimization iterations.

To investigate this, we take the optimized parameters from the Isotropic DD experiments on SMOOTHADV for an initial  $\sigma = 0.25$  on CIFAR-10, and run the optimization step of Isotropic DD for 100 iterations more than its default number of iterations from [10], so as to match the total number of optimization steps between Isotropic DD and ANCER. The histograms of  $\sigma^x$  or  $\sigma_{\min}^x$  and the gap-factor  $r$ , *i.e.* the two factors from the  $\ell_2$  certification results, are presented in Figure 5. While  $\sigma^x$  for Isotropic DD is similar in distribution to ANCER’s  $\sigma_{\min}^x$ , the distribution of the two gaps,  $r(x, \sigma^x)$  and  $r(x, \Sigma^x)$ , are quite different. In particular, the ANCER certification gap is significantly larger when compared to Isotropic DD, and is the main contributor to the improvement in the  $\ell_2$ -ball certificate of ANCER. That is to say, ANCER generates  $\Sigma^x$  that is better aligned with the decision boundaries, and hence increases the confidence of the smooth classifier.

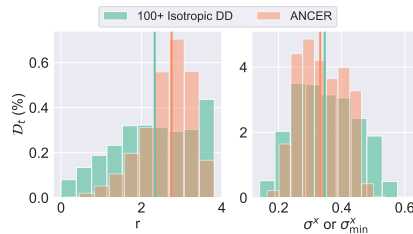


Figure 5: Histograms of the values of the  $\sigma$ -factor (left) and gap  $r$  (right) obtained by ANCER initialized with Isotropic DD, and Isotropic DD when allowed to run for 100 iterations more than the baseline. Vertical lines plot the median of the data.

### 7.4 Visual Comparison of Parameters in Ellipsoid Certificates

Anisotropic certification allows for a better characterization of the decision boundaries of the base classifier  $f$ . For example, the directions aligned with the major axes of the ellipsoids  $\|\delta\|_{\Sigma,2} = r$ , *i.e.* locations where  $\Sigma$  is large, are, by definition, expected to be less sensitive to perturbations compared to the minor axes directions. To visualize this concept, Figure 6 shows CIFAR-10 images along with their corresponding optimized  $\ell_2$  isotropic parameters obtained by Isotropic DD, and  $\ell_2^\Sigma$  anisotropic parameters obtained by ANCER. First, we note the richness of information provided by the anisotropic parameters when compared to the  $\ell_2$  worst-case, isotropic one. Interestingly, pixel locations where the intensity of  $\Sigma$  is large (higher intensity in Figure 6) are generally the ones corresponding least with the underlying true class and overlapping more with background pixels.

### 7.5 Certification Runtime

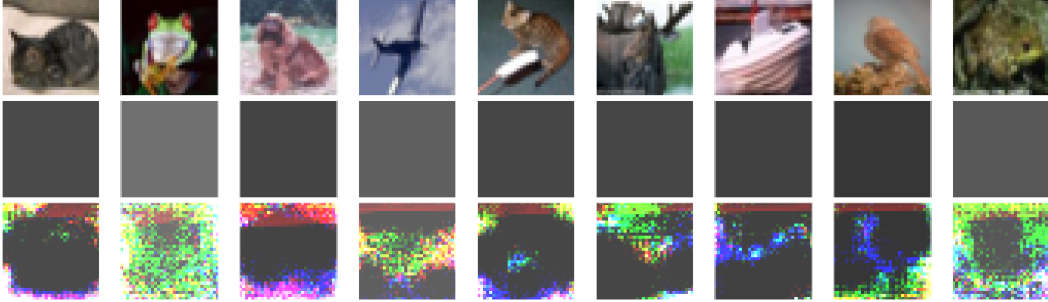


Figure 6: Visualization of an input CIFAR-10 image  $x$  (top), and the optimized parameters  $\sigma$  (middle) and  $\Sigma$  (bottom) – higher intensity corresponds to higher  $\sigma_i$  in that pixel and channel – of the smoothing distributions in the isotropic and anisotropic case, respectively.

The certification procedures of Isotropic DD and ANCER tradeoff improved certified accuracy for runtime, since they require a sample-wise optimization to be run prior to the CERTIFY step described in [5]. The runtime of the optimization and certification procedures is roughly equal for  $\ell_1$ ,  $\ell_2$ ,  $\ell_2^\Sigma$  and  $\ell_1^\Lambda$  certification, and mostly depends on network architecture. As such, we report the certification runtime for a test set sample on an NVIDIA Quadro RTX 6000 GPU for Fixed  $\sigma$ , Isotropic DD and ANCER (including the isotropic initialization step) in Table 3. We observe that the overall run time overhead for ANCER is not significant as compared to its certification gains.

Table 3: Certification time for each sample per architecture used: (a) ResNet18 ( $\ell_2$ ,  $\ell_2^\Sigma$  on CIFAR-10), (b) WideResNet40 ( $\ell_1$ ,  $\ell_1^\Lambda$  on CIFAR-10), and (c) ResNet50 (ImageNet).

	Fixed $\sigma$	Isotropic DD	ANCER
(a)	1.6s	1.7s	2.4s
(b)	7.4s	9.4s	11.4s
(c)	109.5s	135.8s	146.3s

## 8 Conclusion

In this work, we lay the theoretical foundations for anisotropic certification through a simple analysis, propose a metric for comparing general robustness certificates, and introduce ANCER, a certification procedure that estimates the parameters of the anisotropic smoothing distribution to maximize the certificate. Our experiments show that ANCER achieves state-of-the-art  $\ell_1$  and  $\ell_2$  certified accuracy on CIFAR-10 and ImageNet (when limited to an isotropic region), as well as a significant improvement in terms of the volume of the certified region. Our anisotropic analysis enables further insights about the boundary of the safe region around an input sample, as compared to its isotropic counterpart.

## Acknowledgments and Disclosure of Funding

This work was supported by the EPSRC Centre for Doctoral Training in Autonomous Intelligent Machines and Systems [EP/S024050/1] and Five AI Limited; by the King Abdullah University of Science and Technology (KAUST) Office of Sponsored Research (OSR) under Award No. OSR-CRG2019-4033; and by the Royal Academy of Engineering under the Research Chair and Senior Research Fellowships scheme, EPSRC/MURI grant EP/N019474/1 and Five AI Limited.

## References

- [1] Ian Goodfellow, Jonathon Shlens, and Christian Szegedy. Explaining and harnessing adversarial examples. In *International Conference on Learning Representations (ICLR)*, 2015. 1, 2
- [2] Christian Szegedy, Wojciech Zaremba, Ilya Sutskever, Joan Bruna, Dumitru Erhan, Ian Goodfellow, and Rob Fergus. Intriguing properties of neural networks. In *International Conference on Learning Representations (ICLR)*, 2014. 1, 2
- [3] Jia Deng, Wei Dong, Richard Socher, Li-Jia Li, Kai Li, and Li Fei-Fei. Imagenet: A large-scale hierarchical image database. In *IEEE Conference on Computer Vision and Pattern Recognition (CVPR)*, 2009. 1, 2, 6, 18

- [4] Mathias Lecuyer, Vaggelis Atlidakis, Roxana Geambasu, Daniel Hsu, and Suman Jana. Certified robustness to adversarial examples with differential privacy. In *IEEE Symposium on Security and Privacy (SP)*, 2019. 1, 2, 5
- [5] Jeremy M Cohen, Elan Rosenfeld, and J Zico Kolter. Certified adversarial robustness via randomized smoothing. In *International Conference on Machine Learning (ICML)*, 2019. 1, 2, 3, 4, 5, 6, 7, 8, 10, 16, 18, 19
- [6] Greg Yang, Tony Duan, J Edward Hu, Hadi Salman, Ilya Razenshteyn, and Jerry Li. Randomized smoothing of all shapes and sizes. In *International Conference on Machine Learning (ICML)*, 2020. 1, 2, 3, 4, 5, 6, 7, 8, 9, 18, 19
- [7] Aounon Kumar, Alexander Levine, Tom Goldstein, and Soheil Feizi. Curse of dimensionality on randomized smoothing for certifiable robustness. In *International Conference on Machine Learning (ICML)*, 2020.
- [8] Alexander Levine and Soheil Feizi. Improved, deterministic smoothing for l1 certified robustness. *arXiv preprint arXiv:2103.10834*, 2021. 2
- [9] Alex Krizhevsky. Learning multiple layers of features from tiny images. Technical report, 2009. 2, 6, 13, 18
- [10] Motasem Alfarra, Adel Bibi, Philip HS Torr, and Bernard Ghanem. Data dependent randomized smoothing. *arXiv preprint arXiv:2012.04351*, 2020. 2, 3, 6, 7, 8, 9, 13, 16, 18
- [11] Xiaowei Huang, Marta Kwiatkowska, Sen Wang, and Min Wu. Safety verification of deep neural networks. In *International Conference on Computer Aided Verification (CAV)*, 2017. 2
- [12] Sven Gowal, Krishnamurthy Dj Dvijotham, Robert Stanforth, Rudy Bunel, Chongli Qin, Jonathan Uesato, Relja Arandjelovic, Timothy Mann, and Pushmeet Kohli. Scalable verified training for provably robust image classification. In *IEEE International Conference on Computer Vision (ICCV)*, 2019. 2
- [13] Aditi Raghunathan, Jacob Steinhardt, and Percy S Liang. Semidefinite relaxations for certifying robustness to adversarial examples. In *Advances in Neural Information Processing Systems (NeurIPS)*, 2018. 2
- [14] Rudy Bunel, Ilker Turkaslan, Philip HS Torr, Pushmeet Kohli, and M Pawan Kumar. A unified view of piecewise linear neural network verification. In *Advances in Neural Information Processing Systems (NeurIPS)*, 2018. 2
- [15] Alessio Lomuscio and Lalit Maganti. An approach to reachability analysis for feed-forward relu neural networks. *arXiv preprint arXiv:1706.07351*, 2017.
- [16] Hadi Salman, Greg Yang, Huan Zhang, Cho-Jui Hsieh, and Pengchuan Zhang. A convex relaxation barrier to tight robust verification of neural networks. In *Advances in Neural Information Processing Systems (NeurIPS)*, 2019. 2
- [17] Vincent Tjeng, Kai Xiao, and Russ Tedrake. Evaluating robustness of neural networks with mixed integer programming. In *International Conference on Learning Representations (ICLR)*, 2019. 2
- [18] Tsui-Wei Weng, Huan Zhang, Hongge Chen, Zhao Song, Cho-Jui Hsieh, Duane Boning, Inderjit S Dhillon, and Luca Daniel. Towards fast computation of certified robustness for relu networks. In *International Conference on Machine Learning (ICML)*, 2018. 2
- [19] Bai Li, Changyou Chen, Wenlin Wang, and Lawrence Carin. Certified adversarial robustness with additive noise. In *Advances in Neural Information Processing Systems (NeurIPS)*, 2019. 2
- [20] Hadi Salman, Jerry Li, Ilya P Razenshteyn, Pengchuan Zhang, Huan Zhang, Sébastien Bubeck, and Greg Yang. Provably robust deep learning via adversarially trained smoothed classifiers. In *Advances in Neural Information Processing Systems (NeurIPS)*, 2019. 2, 4, 5, 6, 7, 8, 14, 18, 19

- [21] Runtian Zhai, Chen Dan, Di He, Huan Zhang, Boqing Gong, Pradeep Ravikumar, Cho-Jui Hsieh, and Liwei Wang. Macer: Attack-free and scalable robust training via maximizing certified radius. In *International Conference on Learning Representations (ICLR)*, 2019. 2, 4, 5, 6, 7, 8, 18, 19
- [22] Jongheon Jeong and Jinwoo Shin. Consistency regularization for certified robustness of smoothed classifiers. In *Advances in Neural Information Processing Systems (NeurIPS)*, 2020. 2
- [23] Guang-He Lee, Yang Yuan, Shiyu Chang, and Tommi S Jaakkola. Tight certificates of adversarial robustness for randomly smoothed classifiers. *arXiv preprint arXiv:1906.04948*, 2019. 2, 3
- [24] Alexander Levine and Soheil Feizi. Robustness certificates for sparse adversarial attacks by randomized ablation. In *Association for the Advancement of Artificial Intelligence (AAAI)*, 2020. 3
- [25] Dinghuai Zhang, Mao Ye, Chengyue Gong, Zhanxing Zhu, and Qiang Liu. Filling the soap bubbles: Efficient black-box adversarial certification with non-gaussian smoothing. <https://openreview.net/forum?id=Skq8gJBFvr>, 2019. 3
- [26] Krishnamurthy Dj Dvijotham, Jamie Hayes, Borja Balle, Zico Kolter, Chongli Qin, András György, Kai Xiao, Sven Gowal, and Pushmeet Kohli. A framework for robustness certification of smoothed classifiers using f-divergences. In *International Conference on Learning Representations (ICLR)*, 2020. 3
- [27] Hamid Karimi, Tyler Derr, and Jiliang Tang. Characterizing the decision boundary of deep neural networks. *arXiv preprint arXiv:1912.11460*, 2019. 3
- [28] Florian Tramèr, Nicolas Papernot, Ian Goodfellow, Dan Boneh, and Patrick McDaniel. The space of transferable adversarial examples. *arXiv preprint arXiv:1704.03453*, 2017. 3
- [29] Florian Tramèr, Alexey Kurakin, Nicolas Papernot, Ian Goodfellow, Dan Boneh, and Patrick McDaniel. Ensemble adversarial training: Attacks and defenses. In *International Conference on Learning Representations (ICLR)*, 2018. 3
- [30] Marc Fischer, Maximilian Baader, and Martin Vechev. Certified defense to image transformations via randomized smoothing. In *Advances in Neural Information Processing Systems (NeurIPS)*, 2020. 4
- [31] Linyi Li, Maurice Weber, Xiaojun Xu, Luka Rimanic, Tao Xie, Ce Zhang, and Bo Li. Provable robust learning based on transformation-specific smoothing. *arXiv preprint arXiv:2002.12398*, 2020. 4
- [32] Maurice G Kendall. *A Course in the Geometry of n Dimensions*. Courier Corporation, 2004. 5, 15
- [33] Diederik P. Kingma and Jimmy Ba. Adam: A method for stochastic optimization. In *International Conference for Learning Representations (ICLR)*, 2015. 6, 7
- [34] Seyed-Mohsen Moosavi-Dezfooli, Alhussein Fawzi, Jonathan Uesato, and Pascal Frossard. Robustness via curvature regularization, and vice versa. In *IEEE Conference on Computer Vision and Pattern Recognition (CVPR)*, 2019. 13
- [35] Adam Paszke, Sam Gross, Francisco Massa, Adam Lerer, James Bradbury, Gregory Chanan, Trevor Killeen, Zeming Lin, Natalia Gimelshein, Luca Antiga, Alban Desmaison, Andreas Kopf, Edward Yang, Zachary DeVito, Martin Raison, Alykhan Tejani, Sasank Chilamkurthy, Benoit Steiner, Lu Fang, Junjie Bai, and Soumith Chintala. Pytorch: An imperative style, high-performance deep learning library. In *Advances in Neural Information Processing Systems (NeurIPS)*. 2019. 18
- [36] Kaiming He, Xiangyu Zhang, Shaoqing Ren, and Jian Sun. Deep residual learning for image recognition. In *IEEE Conference on Computer Vision and Pattern Recognition*, 2016. 18

## A Visualization on CIFAR-10 of Optimized Isotropic vs. Anisotropic Certification

To extend the illustration in Figure 1 to a higher dimensional input, we now analyze an example of the isotropic  $\ell_2$  certification of randomized smoothing with  $\mathcal{N}(0, \sigma^2 I)$ , where  $\sigma$  is optimized per input [10], against ANCER, certifying an anisotropic region characterized by a diagonal  $\ell_2^\Sigma$ -norm. To do so, we consider a CIFAR-10 [9] dataset point  $x$ , where the input is of size  $(32 \times 32 \times 3)$ . We perform the 2D analysis by considering the regions closest to a decision boundary. To do so, and following [34], we compute the Hessian of  $f^y(x)$  with respect to  $x$  where  $y$  is the true label for  $x$  with  $f$  classifying  $x$  correctly, *i.e.*  $y = \arg \max_i f^i(x)$ . In addition to the Hessian, we also compute its eigenvector decomposition, yielding the eigenvectors  $\{\nu_i\}, i \in \{1, \dots, 3072\}$  ordered in descending order of the absolute value of the respective eigenvalues. In Figure 7a, we show the projection of the landscape of  $f^y$  in the highest curvature directions, *i.e.*  $\nu_1$  and  $\nu_2$ . Note that the isotropic certification, much as in Figure 1c, in these 2 dimensions is nearly optimal when compared to the anisotropic region. However, if we take the same projection with respect to the eigenvectors with the lowest and highest eigenvalues, *i.e.*  $\nu_1$  and  $\nu_{3072}$ , the advantages of the anisotropic certification become clear as shown in Figure 7b.

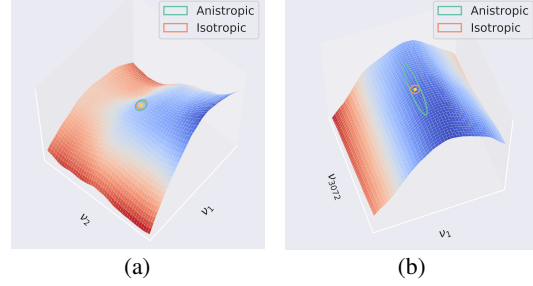


Figure 7: Illustration of the landscape of  $f^y$  for points around an input point  $x$ , and two projections of an isotropic  $\ell_2$  certified region and an anisotropic  $\ell_2^\Sigma$  2-norm region on a CIFAR-10 dataset example to a subset of two eigenvectors of the Hessian of  $f^y$  (blue regions correspond to a higher confidence in  $y$ ).

## B Anisotropic Certification and Evaluation Proofs

**Proposition 1** (restatement). *Consider a differentiable function  $g : \mathbb{R}^n \rightarrow \mathbb{R}$ . If  $\sup_x \|\nabla g(x)\|_* \leq L$  where  $\|\cdot\|_*$  has a dual norm  $\|z\| = \max_x z^\top x$  s.t.  $\|x\|_* \leq 1$ , then  $g$  is  $L$ -Lipschitz under norm  $\|\cdot\|_*$ , that is  $|g(x) - g(y)| \leq L\|x - y\|$ .*

*Proof.* Consider some  $x, y \in \mathbb{R}^n$  and a parameterization in  $t$  as  $\gamma(t) = (1-t)x + ty \ \forall t \in [0, 1]$ . Note that  $\gamma(0) = x$  and  $\gamma(1) = y$ . By the Fundamental Theorem of Calculus we have:

$$\begin{aligned} |g(y) - g(x)| &= |g(\gamma(1)) - g(\gamma(0))| = \left| \int_0^1 \frac{dg(\gamma(t))}{dt} dt \right| = \left| \int_0^1 \nabla g^\top \nabla \gamma dt \right| \leq \int_0^1 |\nabla g^\top \nabla \gamma| dt \\ &\leq \int_0^1 \|\nabla g(x)\|_* \|\nabla \gamma(t)\| dt \leq L\|y - x\| \end{aligned}$$

□

**Theorem 1** (restatement). *Let  $g : \mathbb{R}^n \rightarrow \mathbb{R}^K$ ,  $g^i$  be  $L$ -Lipschitz continuous under norm  $\|\cdot\|_*$ ,  $\forall i \in \{1, \dots, K\}$ , and  $c_A = \arg \max_i g^i(x)$ . Then, we have  $\arg \max_i g^i(x + \delta) = c_A$  for all  $\delta$  satisfying:*

$$\|\delta\| \leq \frac{1}{2L} \left( g^{c_A}(x) - \max_c g^{c \neq c_A}(x) \right).$$

*Proof.* Take  $c_B = \arg \max_c g^{c \neq c_A}(x)$ . By Proposition 1, we get:

$$\begin{aligned} |g^{c_A}(x + \delta) - g^{c_A}(x)| &\leq L\|\delta\| \implies g^{c_A}(x + \delta) \geq g^{c_A}(x) - L\|\delta\| \\ |g^{c_B}(x + \delta) - g^{c_B}(x)| &\leq L\|\delta\| \implies g^{c_B}(x + \delta) \leq g^{c_B}(x) + L\|\delta\| \end{aligned}$$

By subtracting the inequalities and re-arranging terms, we have that as long as  $g^{c_A}(x) - L\|\delta\| > g^{c_B}(x) + L\|\delta\|$ , *i.e.* the bound in the Theorem, then  $g^{c_A}(x + \delta) > g^{c_B}(x + \delta)$ , completing the proof. □



**Proposition 2** (restatement). Consider  $g_\Sigma(x) = \mathbb{E}_{\epsilon \sim \mathcal{N}(0, \Sigma)} [f(x + \epsilon)]$ .  $\Phi^{-1}(g_\Sigma(x))$  is 1-Lipschitz (i.e.  $L = 1$ ) under the  $\|\cdot\|_{\Sigma^{-1}, 2}$  norm.

*Proof.* To prove Proposition 2, one needs to show that  $g_\Sigma^i(x) \forall i$  is 1-Lipschitz under the  $\|\cdot\|_{\Sigma^{-1}, 2}$  norm. For ease of notation, we drop the superscript  $g_\Sigma^i$  and use only  $g$ . We want to show that  $\|\nabla \Phi^{-1}(g_\Sigma(x))\|_{\Sigma^{-1}, 2} = \|\Sigma^{1/2} \nabla \Phi^{-1}(g_\Sigma(x))\|_2 \leq 1$ . Following the argument presented in [20], it suffices to show that, for any unit norm direction  $u$  and  $p = g_\Sigma(x)$ , we have:

$$u^\top \Sigma^{\frac{1}{2}} \nabla g_\Sigma(x) \leq \frac{1}{\sqrt{2\pi}} \exp\left(-\frac{1}{2}(\Phi^{-1}(p))^2\right). \quad (2)$$

We start by noticing that:

$$\begin{aligned} u^\top \Sigma^{\frac{1}{2}} \nabla g_\Sigma(x) &= \frac{1}{(\sqrt{2\pi})^n \sqrt{|\Sigma|}} \int_{\mathbb{R}^n} f(t) u^\top \Sigma^{\frac{1}{2}} \Sigma^{-1}(t-x) \exp\left(-\frac{1}{2}(x-t)\Sigma^{-1}(x-t)\right) d^n t \\ &= \mathbb{E}_{s \sim \mathcal{N}(0, \mathbf{I})} [f(x + \Sigma^{\frac{1}{2}} s) u^\top s] = \mathbb{E}_{v \sim \mathcal{N}(0, \Sigma)} [f(x+v) u^\top \Sigma^{-\frac{1}{2}} v]. \end{aligned}$$

We now want to show that the function  $f : \mathbb{R}^n \rightarrow [0, 1]$ , note that  $f$  is the function to be smoothed that maps to a probability simplex, which **(i)** satisfies  $g_\Sigma(x) = \mathbb{E}_{v \sim \mathcal{N}(0, \Sigma)} [f(x+v)] = p$  while **(ii)** maximizing  $\mathbb{E}_{v \sim \mathcal{N}(0, \Sigma)} [f(x+v) u^\top \Sigma^{-\frac{1}{2}} v]$  is given by:

$$f^*(x+v) = \mathbb{1} \left\{ u^\top \Sigma^{-\frac{1}{2}} v \geq -\Phi^{-1}(p) \right\}.$$

To prove that  $f^*$  is the optimal solution we first show feasibility. **(i)**: It is clear that  $f^* : \mathbb{R}^n \rightarrow [0, 1]$ , and note that **(ii)**:

$$\mathbb{E}_{v \sim \mathcal{N}(0, \Sigma)} \left[ \mathbb{1} \left\{ u^\top \Sigma^{-\frac{1}{2}} v \geq -\Phi^{-1}(p) \right\} \right] = \mathbb{P}_{x \sim \mathcal{N}(0, 1)} (x \geq -\Phi^{-1}(p)) = 1 - \Phi(-\Phi^{-1}(p)) = p.$$

At last, we show that  $f^*$  attains the upper bound **(ii)**:

$$\begin{aligned} \mathbb{E}_{v \sim \mathcal{N}(0, \Sigma)} \left[ u^\top \Sigma^{-\frac{1}{2}} v \mathbb{1} \left\{ u^\top \Sigma^{-\frac{1}{2}} v \geq -\Phi^{-1}(p) \right\} \right] &= \mathbb{E}_{x \sim \mathcal{N}(0, 1)} \left[ x \mathbb{1} \{x \geq -\Phi^{-1}(p)\} \right] \\ &= \frac{1}{\sqrt{2\pi}} \int_{-\Phi^{-1}(p)}^{\infty} x \exp\left(-\frac{1}{2}x^2\right) dx \\ &= \frac{1}{\sqrt{2\pi}} \exp\left(-\frac{1}{2}(\Phi^{-1}(p))^2\right) \end{aligned}$$

obtaining the bound from Equation (2), and thus completing the proof.  $\square$

**Proposition 3** (restatement). Consider  $g_\Lambda(x) = \mathbb{E}_{\epsilon \sim \mathcal{U}[-1, 1]^n} [f(x + \Lambda\epsilon)]$ . The classifier  $g_\Lambda^i \forall i$  is  $1/2$ -Lipschitz (i.e.  $L = 1/2$ ) under the  $\|\Lambda x\|_\infty$  norm.

*Proof.* We begin by observing that the dual norm of  $\|x\|_{\Lambda, 1} = \|\Lambda^{-1}x\|_1$  is  $\|x\|_* = \|\Lambda x\|_\infty$ , since:

$$\max_{\|\Lambda^{-1}x\|_1 \leq 1} x^T y = \max_{\|z\|_1 \leq 1} y^T \Lambda z = \|\Lambda y\|_\infty.$$

Without loss of generality, we analyze  $\partial g^i / \partial x_1$ . Let  $\hat{x} = [x_2, \dots, x_n] \in \mathbb{R}^{n-1}$ , then:

$$\begin{aligned} \frac{\lambda_1 \partial g^i}{\partial x_1} &= \frac{\lambda_1}{(2\lambda)^n} \frac{\partial}{\partial x_1} \int_{[-1, 1]^{n-1}} \int_{-1}^1 f^i(x_1 + \lambda_1 \epsilon_1, \hat{x} + \hat{\Lambda} \hat{\epsilon}) d\epsilon_1 d^{n-1} \hat{\epsilon} \\ &= \frac{1}{2^n} \int_{[-1, 1]^{n-1}} (f^i(x_1 + 1, \hat{x} + \hat{\Lambda} \hat{\epsilon}) - f^i(x_1 - 1, \hat{x} + \hat{\Lambda} \hat{\epsilon})) d^{n-1} \hat{\epsilon} \end{aligned}$$

Thus,

$$\left| \frac{\lambda_1 \partial g^i}{\partial x_1} \right| \leq \frac{1}{2^n \prod_{j=2}^n \lambda_j} \int_{[-1, 1]^{n-1}} \left| f^i(x_1 + 1, \hat{x} + \hat{\Lambda} \hat{\epsilon}) - f^i(x_1 - 1, \hat{x} + \hat{\Lambda} \hat{\epsilon}) \right| d^{n-1} \hat{\epsilon} \leq \frac{1}{2}.$$

The second and last steps follow by the change of variable  $t = x_1 + \lambda_1 \epsilon_1$  and Leibniz rule. Following a symmetric argument,  $|\lambda_j \partial g^i / \partial x_j| \leq 1/2 \forall i$  resulting in having  $\|\Lambda \nabla g^i(x)\|_\infty = \max_i \lambda_i |\partial g^i / \partial x_i| \leq 1/2 \forall i$  concluding the proof.  $\square$

**Proposition 4** (restatement).  $\mathcal{V}(\{\delta : \|\Lambda^{-1}\delta\|_1 \leq r\}) = \frac{(2r)^n}{n!} \prod_i \lambda_i$ .

*Proof.* Take  $A = r\Lambda^{-1} = \text{diag}(1/r\lambda_1, \dots, 1/r\lambda_n) = \text{diag}(a_1, \dots, a_n)$ .

We can re-write the region as  $\{x : \sum_i a_i |x_i| \leq 1\}$ , from which it is clear to see that this region is an origin centered, axis-aligned simplex with the set of vertices  $\mathcal{V} = \{\pm 1/a_i \mathbf{e}_i\}_{i=1}^n$ , where  $\mathbf{e}_i$  is the standard basis vector  $i$ .

Define the sets of vertices  $\mathcal{V}^t = \mathcal{V} \setminus \{-1/a_n \mathbf{e}_n\}$  and  $\mathcal{V}^b = \mathcal{V} \setminus \{1/a_n \mathbf{e}_n\}$ . Given the symmetry around the origin, each of these sets defines an  $n$ -dimensional *hyperpyramid* with a shared *base*  $B_{n-1}$  given by the  $n-1$ -dimensional hyperplane defined by all vertices where  $x_n = 0$ , and an *apex* at the vertex  $1/a_n \mathbf{e}_n$  (or  $-1/a_n \mathbf{e}_n$  in the case of  $\mathcal{V}^b$ ). The volume of each of these  $n-1$ -dimensional hyperpyramids is given by  $\mathcal{V}^{(B_{n-1})/na_n}$  ([32]), yielding a total volume of  $V_n = \frac{2}{n} \frac{1}{a_n} \mathcal{V}(B_{n-1})$ . The same argument can be applied to compute  $\mathcal{V}(B_{n-1})$  which is a union of two  $n-1$ -dimensional hyperpyramids. This forms a recursion that completes the proof.  $\square$

*Proof. (Alternative Proof.)* We consider the case that  $\Lambda^{-1}$  is a general positive definite matrix that is not necessarily diagonal. Note that  $\mathcal{V}(\{\delta : \|\Lambda^{-1}\delta\|_1 \leq r\}) = \mathcal{V}(\{\delta : \|(r\Lambda)^{-1}\delta\|_1 \leq 1\}) = r^n |\Lambda| \mathcal{V}(\{\delta : \|\delta\|_1 \leq 1\})$  where  $|r\Lambda|$  denotes the determinant. The last equality follows by the volume of a set under a linear map and noting that  $\{\delta : \|(r\Lambda)^{-1}\delta\|_1 \leq 1\} = \{r\Lambda\delta : \|\delta\|_1 \leq 1\}$ . At last,  $\{\delta : \|\delta\|_1 \leq 1\}$  can be expressed as the disjoint union of  $2^n$  simplexes. Thus, we have  $\mathcal{V}(\{\delta : \|\Lambda^{-1}\delta\|_1 \leq r\}) = (2r)^n / n! |\Lambda|$  since the volume of a simplex is  $1/n!$  completing the proof.  $\square$

For completeness, we supplemental the previous result with a bound on the volume that may be useful for future readers.

**Proposition 5.** For any positive definite  $\Lambda^{-1} \in \mathbb{R}^{n \times n}$ , we have the following:

$$\left(\frac{2r}{n}\right)^n \mathcal{V}(\mathcal{Z}(\Lambda)) \leq \mathcal{V}(\{\delta : \|\Lambda^{-1}\delta\|_1 \leq r\}) \leq (2r)^n \mathcal{V}(\mathcal{Z}(\Lambda))$$

where  $\mathcal{V}(\mathcal{Z}(\Lambda)) = \sqrt{|\Lambda^\top \Lambda|}$  which is the volume of the zonotope with a generator matrix  $\Lambda$ .

*Proof.* Let  $S_1 = \{\delta : \|\Lambda^{-1}\delta\|_1 \leq r\}$ ,  $S_\infty = \{\delta : \|\Lambda^{-1}\delta\|_\infty \leq r\}$  and  $S_\infty^n = \{\delta : n\|\Lambda^{-1}\delta\|_\infty \leq r\}$ . Since  $\|\Lambda^{-1}\delta\|_\infty \leq \|\Lambda^{-1}\delta\|_1 \leq n\|\Lambda^{-1}\delta\|_\infty$ , then  $S_\infty \supseteq S_1 \supseteq S_\infty^n$ . Therefore, we have  $\mathcal{V}(S_\infty) \geq \mathcal{V}(S_1) \geq \mathcal{V}(S_\infty^n)$ . At last note that,  $S_\infty^n = \{\frac{r}{n}\Lambda\delta : \|\delta\|_\infty \leq 1\}$  and that with the change of variables  $\delta = 2u - 1_n$  where  $1_n$  is a vector of all ones, we have  $S_\infty^n = \mathcal{Z}\left(\frac{2r}{n}\Lambda\right) \oplus \frac{-r}{n}\Lambda 1_n$  where  $\oplus$  is a Minkowski sum and noting that  $\frac{r}{n}\Lambda 1_n$  is a single point in  $\mathbb{R}^n$ . Therefore,  $\mathcal{V}\left(\mathcal{Z}\left(\frac{2r}{n}\Lambda\right) \oplus \frac{-r}{n}\Lambda 1_n\right) = (2r/n)^n \mathcal{V}(\mathcal{Z}(\Lambda))$ . The upper bound follows with a similar argument completing the proof.  $\square$

## B.1 Certification under Gaussian Mixture Smoothing Distribution

We consider a general,  $K$ -component, zero-mean Gaussian mixture smoothing distribution  $\mathcal{G}$  such that:

$$\mathcal{G}(\{\alpha_i, \Sigma_i\}_{i=1}^K) := \sum_{i=1}^K \alpha_i \mathcal{N}(0, \Sigma_i), \quad \text{s.t.} \quad \sum_i \alpha_i = 1, 0 < \alpha_i \leq 1 \quad (3)$$

Given  $f$  and as per the recipe described in Section 4, we are interested in the Lipschitz constant of the smooth classifier  $g_{\mathcal{G}}(x) = (f * \mathcal{G})(x) = \sum_i^K \alpha_i g_{\Sigma_i} = \sum_i^K \alpha_i (f * \mathcal{N}(0, \Sigma_i)) = \sum_i \alpha_i g_{\Sigma_i}(x)$  where  $g_{\Sigma_i}$  is defined as in the Gaussian case.

Note the weaker bound when compared to Proposition 2, for each of the Gaussian components presented in the following proposition.

**Proposition 6.**  $g_{\Sigma}$  is  $\sqrt{2/\pi}$ -Lipschitz under  $\|\cdot\|_{\Sigma^{-1}, 2}$  norm.

*Proof.* Following a similar argument to the proof of Proposition 2, we get:

$$\begin{aligned} u^\top \Sigma^{\frac{1}{2}} \nabla g_{\Sigma}(x) &\leq \frac{1}{(2\pi)^{n/2} \sqrt{|\Sigma|}} \int_{\mathbb{R}^n} |u^\top \Sigma^{-\frac{1}{2}}(t-x)| \exp\left(-\frac{1}{2}(x-t)^\top \Sigma^{-1}(x-t)\right) d^n t \\ &= \mathbb{E}_{s \sim \mathcal{N}(0, \mathbf{I})} [ |u^\top s| ] = \mathbb{E}_{v \sim \mathcal{N}(0, 1)} [|v|] = \sqrt{2/\pi}. \end{aligned}$$

□

With Proposition 6, we obtain a Lipschitz constant for a Gaussian mixture smoothing distribution as:

**Proposition 7.**  $g_{\mathcal{G}}$  is  $\sqrt{\pi/2}$ -Lipschitz under  $\|\delta\|_{\mathcal{B}^{-1},2}$  norm, where  $\mathcal{B}^{-1} = \sum_i^K \alpha_i \Sigma_i^{-1}$ .

*Proof.*

$$\begin{aligned} |g_{\mathcal{G}}(x + \delta) - g_{\mathcal{G}}(x)| &\leq \sum_i \alpha_i |g_{\Sigma_i}(x + \delta) - g_{\Sigma_i}(x)| \\ &\leq \sqrt{\frac{\pi}{2}} \sum_i \alpha_i \|\delta\|_{\Sigma_i,2} \leq \sqrt{\frac{\pi}{2}} \sqrt{\delta^\top \left( \sum_i \alpha_i \Sigma_i^{-1} \right) \delta} = \sqrt{\frac{\pi}{2}} \|\delta\|_{\mathcal{B},2}, \end{aligned}$$

Obtained by first applying the triangle inequality, then Proposition 2 followed by Jensen’s inequality. □

Thus yielding the following certificate by combining Proposition 7 and Theorem 1.

**Corollary 3.** Let  $c_A = \arg \max_i g_{\mathcal{G}}^i(x)$ , then  $\arg \max_i g_{\mathcal{G}}^i(x + \delta) = c_A$  for all  $\delta$  satisfying:

$$\|\delta\|_{\mathcal{B},2} \leq \frac{1}{\sqrt{2\pi}} \left( g_{\mathcal{G}}^{c_A}(x) - \max_c g_{\mathcal{G}}^{c \neq c_A}(x) \right).$$

where  $\mathcal{B}^{-1} = \sum_i^K \alpha_i \Sigma_i^{-1}$ .

## C ANCER Optimization

In this section we detail the implementation choices required to solving Equation (1). For ease of presentation, we restate the ANCER optimization problem (with  $\Theta^x = \text{diag}(\{\theta_i^x\}_{i=1}^n)$ ):

$$\arg \max_{\Theta^x} r^p(x, \Theta^x) \sqrt[n]{\prod_i \theta_i^x} \quad \text{s.t.} \quad \min_i \theta_i^x r^p(x, \Theta^x) \geq r_{\text{iso}}^*,$$

where  $r^p(x, \Theta^x)$  is the gap value under the anisotropic smoothing distribution, and  $r_{\text{iso}}^*$  is the optimal isotropic radius, i.e.  $\bar{\theta}^x r^p(x, \bar{\theta}^x)$  for  $\bar{\theta}^x \in \mathbb{R}^+$ . This is a nonlinear constrained optimization problem that is challenging to solve. As such, we relax it, and solve instead:

$$\arg \max_{\Theta^x} r^p(x, \Theta^x) \sqrt[n]{\prod_i \theta_i^x} + \kappa \min_i \theta_i^x r^p(x, \Theta^x) \quad \text{s.t.} \quad \theta_i^x \geq \bar{\theta}^x$$

given a hyperparameter  $\kappa \in \mathbb{R}^+$ . While the constraint  $\theta_i^x \geq \bar{\theta}^x$  is not explicitly required to enforce the *superset* condition over the isotropic case, it proved itself beneficial from an empirical perspective. To sample from the distribution parameterized by  $\Theta^x$  (in our case, either a Gaussian or Uniform), we make use of the *reparameterization trick*, as in [10]. The solution of this optimization problem can be found iteratively by performing projected gradient ascent.

A standalone implementation for the ANCER optimization stage is presented in Listing 1, whereas the full code integrated in our code base is available as supplementary material. To perform certification, we simply feed the output of this optimization to the certification procedure from [5].

```
import torch
from torch.autograd import Variable
from torch.distributions.normal import Normal

class Certificate():
    def compute_proxy_gap(self, logits: torch.Tensor):
        raise NotImplementedError

    def sample_noise(self, batch: torch.Tensor, repeated_theta: torch.Tensor):
        raise NotImplementedError

    def compute_gap(self, pABar: float):
```

```

        raise NotImplementedError

class L2Certificate(Certificate):
    def __init__(self, batch_size: int, device: str = "cuda:0"):
        self.m = Normal(torch.zeros(batch_size).to(device),
                        torch.ones(batch_size).to(device))
        self.device = device
        self.norm = "l2"

    def compute_proxy_gap(self, logits: torch.Tensor):
        return self.m.icdf(logits[:, 0].clamp_(0.001, 0.999)) - \
            self.m.icdf(logits[:, 1].clamp_(0.001, 0.999))

    def sample_noise(self, batch: torch.Tensor, repeated_theta: torch.Tensor):
        return torch.randn_like(batch, device=self.device) * repeated_theta

    def compute_gap(self, pABar: float):
        return norm.ppf(pABar)

class L1Certificate(Certificate):
    def __init__(self, device="cuda:0"):
        self.device = device
        self.norm = "l1"

    def compute_proxy_gap(self, logits: torch.Tensor):
        return logits[:, 0] - logits[:, 1]

    def sample_noise(self, batch: torch.Tensor, repeated_theta: torch.Tensor):
        return 2 * (torch.rand_like(batch, device=self.device) - 0.5) * repeated_theta

    def compute_gap(self, pABar: float):
        return 2 * (pABar - 0.5)

def ancer_optimization(
    model: torch.nn.Module, batch: torch.Tensor,
    certificate: Certificate, learning_rate: float,
    isotropic_theta: torch.Tensor, iterations: int,
    samples: int, kappa: float, device: str = "cuda:0"):
    """Optimize batch using ANCER, assuming isotropic initialization point.

    Args:
        model: trained network
        batch: inputs to certify around
        certificate: instance of desired certification object
        learning_rate: optimization learning rate for ANCER
        isotropic_theta: initialization isotropic value per input in batch
        iterations: number of iterations to run the optimization
        samples: number of samples per input and iteration
        kappa: relaxation hyperparameter
    """
    batch_size = batch.shape[0]
    img_size = np.prod(batch.shape[1:])

    # define a variable, the optimizer, and the initial sigma values
    theta = Variable(isotropic_theta, requires_grad=True).to(device)
    optimizer = torch.optim.Adam([theta], lr=learning_rate)
    initial_theta = theta.detach().clone()

    # reshape vectors to have ``samples`` per input in batch
    new_shape = [batch_size * samples]
    new_shape.extend(batch[0].shape)
    new_batch = batch.repeat((1, samples, 1, 1)).view(new_shape)

    # solve iteratively by projected gradient ascend
    for _ in range(iterations):
        theta_repeated = theta.repeat(1, samples, 1, 1).view(new_shape)

        # Reparameterization trick
        noise = certificate.sample_noise(new_batch, theta_repeated)
        out = model(
            new_batch + noise
        ).reshape(batch_size, samples, -1).mean(dim=1)

        vals, _ = torch.topk(out, 2)
        gap = certificate.compute_proxy_gap(vals)

        prod = torch.prod(
            (theta.reshape(batch_size, -1))**(1/img_size), dim=1)

```

```

proxy_radius = prod * gap

radius_maximizer = - (
    proxy_radius.sum() +
    kappa *
    (torch.min(theta.view(batch_size, -1), dim=1).values*gap).sum()
)
radius_maximizer.backward()
optimizer.step()

# project to the initial theta
with torch.no_grad():
    torch.max(theta, initial_theta, out=theta)

return theta

```

Listing 1: Python implementation of the ANCER optimization routine using PyTorch [35]

## D Experimental Setup

The experiments reported in the paper used the CIFAR-10 [9]<sup>4</sup> and ImageNet [3]<sup>5</sup> datasets, and trained ResNet18, WideResNet40 and ResNet50 networks [36]. Experiments used the typical data split for these datasets found in the PyTorch implementation [35]. The procedures to obtain the baseline networks used in the experiments are detailed in Appendix D.1 and D.2 for ellipsoids and generalized cross-polytopes, respectively. Source code to reproduce the ANCER optimization and certification results of this paper is available as supplementary material.

**Isotropic DD Optimization.** We used the available code of [10]<sup>6</sup> to obtain the isotropic data dependent smoothing parameters. To train our models from scratch, we used an adapted version of the code provided in the same repository.

**Certification.** Following [5, 20, 21, 6, 10], all results were certified with  $N_0 = 100$  Monte Carlo samples for selection and  $N = 100,000$  estimation samples, with failure a probability of  $\alpha = 0.001$ .

### D.1 Ellipsoid certification baseline networks

In terms of ellipsoid certification, the baselines we considered were COHEN [5]<sup>7</sup>, SMOOTHADV [20]<sup>8</sup> and MACER [21]<sup>9</sup>.

In the CIFAR-10 experiments, we used a ResNet18 architecture, instead of the ResNet110 used in [5, 20, 21] due to constraints at the level of computation power. As such, we had to train each of the networks from scratch following the procedures available in the source code of each of the baselines. We did so under our own framework, and the training scripts are available in the supplementary material. For the ImageNet experiments we used the ResNet50 networks provided by each of the baselines in their respective open source repositories.

We trained the ResNet18 networks for 120 epochs, with a batch size of 256 and stochastic gradient descent with a learning rate of  $10^{-2}$ , and momentum of 0.9.

### D.2 Generalized Cross-Polytope certification baseline networks

For the certification of generalized cross-polytopes we considered RS4A [6]<sup>10</sup>. As described in RS4A [6], we take  $\lambda = \sigma/\sqrt{3}$  and report results as a function of  $\sigma$  for ease of comparison.

As with the baseline, we ran experiments on CIFAR-10 on a WideResNet40 architecture, and ImageNet on a ResNet50 [6]. However, due to limited computational power, we were not able

<sup>4</sup>Available [here \(url\)](#), under an MIT license.

<sup>5</sup>Available [here \(url\)](#), terms of access detailed in the Download page.

<sup>6</sup>Data Dependent Randomized Smoothing source code available [here](#)

<sup>7</sup>COHEN source code available [here](#).

<sup>8</sup>SMOOTHADV source code available [here](#).

<sup>9</sup>MACER source code available [here](#).

<sup>10</sup>RS4A source code available [here](#).



to run experiments on the wide range of distributional parameters the original work considers, *i.e.*  $\sigma = \{0.15, 0.25, 0.5, 0.75, 1.0, 1.125, 1.5, 1.75, 2.0, 2.25, 2.5, 2.75, 3.0, 3.25, 3.5\}$  on CIFAR-10 and  $\sigma = \{0.25, 0.5, 0.75, 1.0, 1.125, 1.5, 1.75, 2.0, 2.25, 2.5, 2.75, 3.0, 3.25, 3.5\}$  on ImageNet. Instead, and matching the requirements from the ellipsoid section, we choose a subset of  $\sigma = \{0.25, 0.5, 1.0\}$  and performed our analysis at that level.

While the trained models are available in the source code of RS4A, we ran into several issues when we attempted to use them, the most problematic of which being the fact that the clean accuracy of such models was very low in both the WideResNet40 and ResNet50 ones. To avoid these issues we trained the models from scratch, but using the stability training loss as presented in the source code of RS4A. All of these models achieved clean accuracy of over 70%.

Following the procedures described in the original work, we trained the WideResNet40 models with the stability loss used in [6] for 120 epochs, with a batch size of 128 and stochastic gradient descent with a learning rate of  $10^{-2}$ , and momentum of 0.9, along with a step learning rate scheduler with a  $\gamma$  of 0.1. For the ResNet50 networks on ImageNet, we trained them from scratch with stability loss for 90 epochs with a learning rate of 0.1 that drops by a factor of 0.1 after each 30 epochs and a batch size of 256.

## E Superset argument

The results we present in Section 7 support the argument that ANCER achieves, in general, a certificate that is a *superset* of the Fixed  $\sigma$  and Isotropic DD ones. To confirm this at an individual test set sample level, we compare the  $\ell_2$ ,  $\ell_1$ ,  $\ell_2^\Sigma$  and  $\ell_1^\Lambda$  certification results across the different methods, and obtain the percentage of the test set in which ANCER performs at least as well as all other methods in each certificates of the samples. Results of this analysis are presented in Tables 4 and 5.

For most networks and datasets, we observe that ANCER achieves a larger  $\ell_p$  certificate than the baselines in a significant portion of the dataset, showcasing the fact that it obtains a superset of the isotropic region per sample. This is further confirmed by the comparison with the anisotropic certificates, in which, for all trained networks except MACER in CIFAR-10, ANCER’s certificate is superior in over 90% of the test set samples.

Table 4: Superset in top-1  $\ell_2$  and  $\ell_2^\Sigma$  (rounded to nearest percent)

	% ANCER $\ell_2$ is the best	% ANCER $\ell_2^\Sigma$ is the best
CIFAR-10: COHEN	83	93
CIFAR-10: SMOOTHADV	73	90
CIFAR-10: MACER	50	69
ImageNet: COHEN	94	96
ImageNet: SMOOTHADV	90	93

Table 5: Superset in top-1  $\ell_1$  and  $\ell_1^\Lambda$  (rounded to nearest percent)

	% ANCER $\ell_1$ is the best	% ANCER $\ell_1^\Lambda$ is the best
CIFAR-10: RS4A	100	100
ImageNet: RS4A	97	99

## F Experimental Results per $\sigma$

### F.1 Certifying Ellipsoids - $\ell_2$ and $\ell_2^\Sigma$ certification results per $\sigma$

In this section we report certified accuracy at various  $\ell_2$  radii and  $\ell_2^\Sigma$  proxy radii, following the metrics defined in Section 7, for each training method (COHEN [5], SMOOTHADV [20] and MACER [21]), dataset (CIFAR-10 and ImageNet) and  $\sigma$  ( $\sigma \in \{0.12, 0.25, 0.5, 1.0\}$ ). Figures 8 and 9 shows certified accuracy at different  $\ell_2$  radii for CIFAR-10 and ImageNet, respectively, whereas Figures 10 and 11 plot certified accuracy and different  $\ell_2^\Sigma$  proxy radii for CIFAR-10 and ImageNet, respectively.

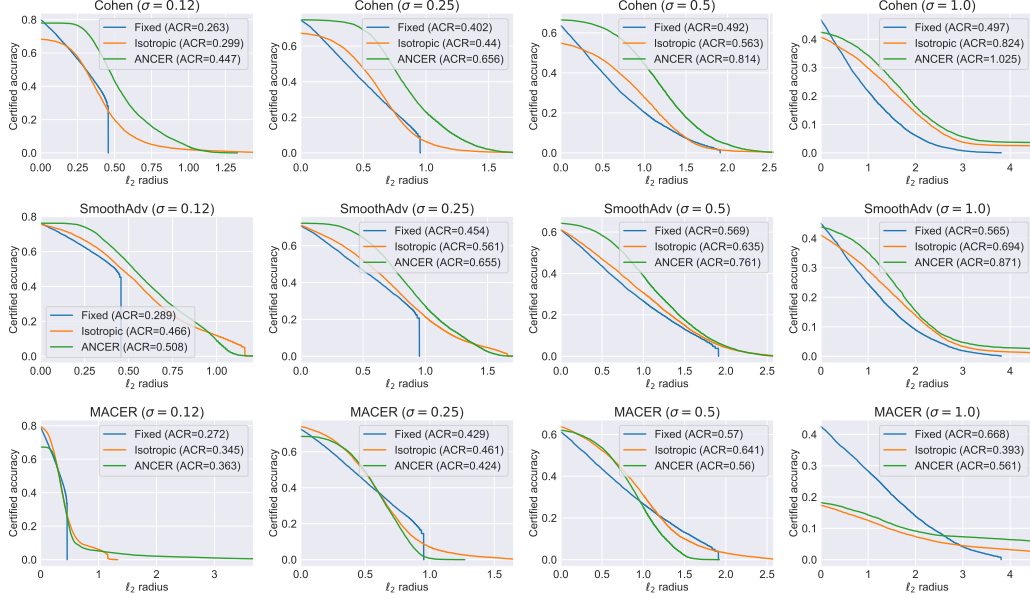


Figure 8: CIFAR-10 certified accuracy as a function of  $\ell_2$  radius, per model and  $\sigma$  (used as initialization in the isotropic data-dependent case and ANCER).

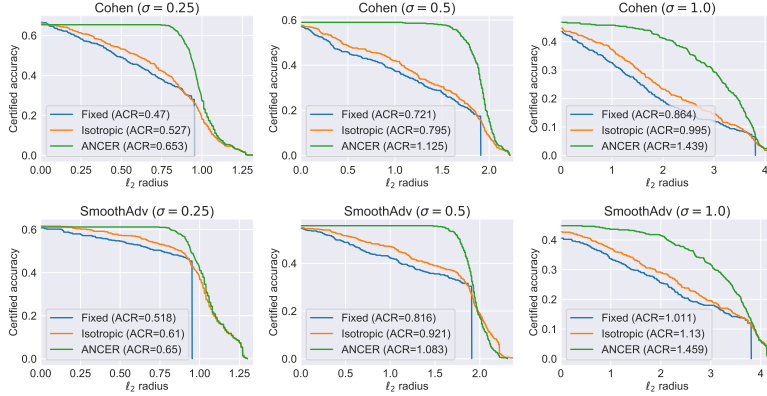


Figure 9: ImageNet certified accuracy as a function of  $\ell_2$  radius, per model and  $\sigma$  (used as initialization in the isotropic data-dependent case and ANCER).

## F.2 Certifying Ellipsoids - $\ell_1$ and $\ell_1^\Delta$ certification results per $\sigma$

In this section we report certified accuracy at various  $\ell_1$  radii and  $\ell_1^\Delta$  proxy radii, following the metrics defined in Section 7, for RS4A, dataset (CIFAR-10 and ImageNet) and  $\sigma$  ( $\sigma \in \{0.25, 0.5, 1.0\}$ ). Figures 12 and 13 shows certified accuracy at different  $\ell_1$  radii for CIFAR-10 and ImageNet, respectively, whereas Figures 14 and 15 plot certified accuracy and different  $\ell_1^\Delta$  proxy radii for CIFAR-10 and ImageNet, respectively.

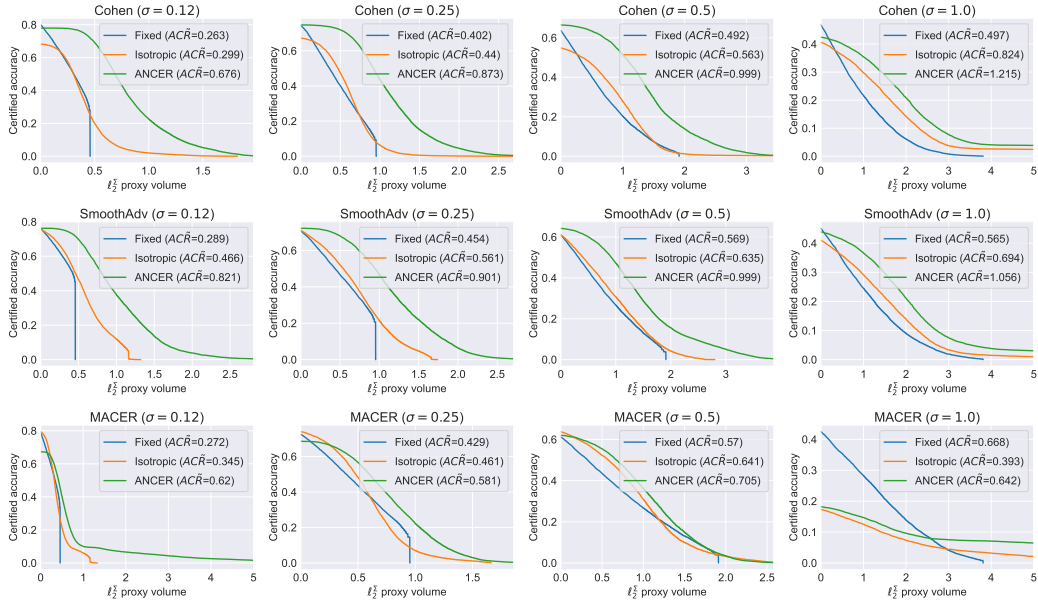


Figure 10: CIFAR-10 certified accuracy as a function of  $\ell_2^2$  proxy radius, per model and  $\sigma$  (used as initialization in the isotropic data-dependent case and ANCER).

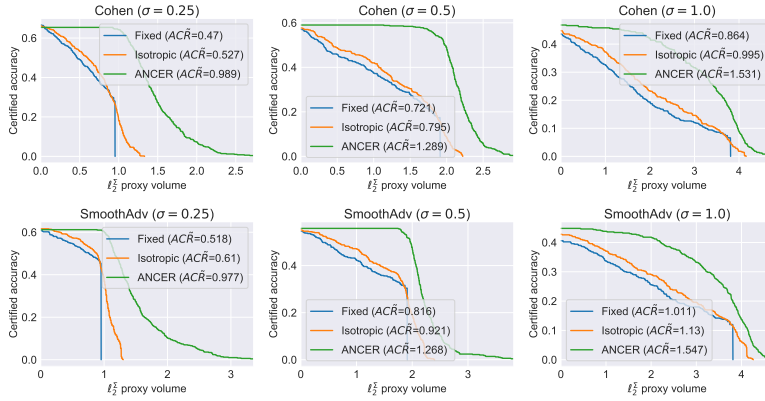


Figure 11: ImageNet certified accuracy as a function of  $\ell_2^2$  proxy radius, per model and  $\sigma$  (used as initialization in the isotropic data-dependent case and ANCER).

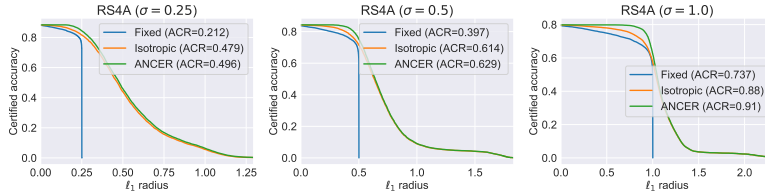


Figure 12: CIFAR-10 certified accuracy as a function of  $\ell_1$  radius per  $\sigma$  (used as initialization in the isotropic data-dependent case and ANCER).

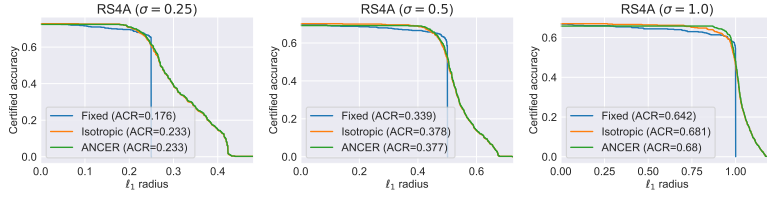


Figure 13: ImageNet certified accuracy as a function of  $\ell_1$  radius per  $\sigma$  (used as initialization in the isotropic data-dependent case and ANCER).

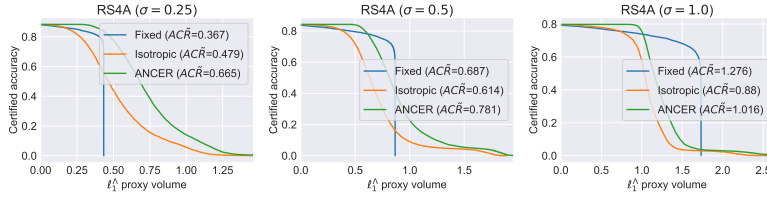


Figure 14: CIFAR-10 certified accuracy as a function of  $\ell_1^\Lambda$  proxy radius per  $\sigma$  (used as initialization in the isotropic data-dependent case and ANCER).

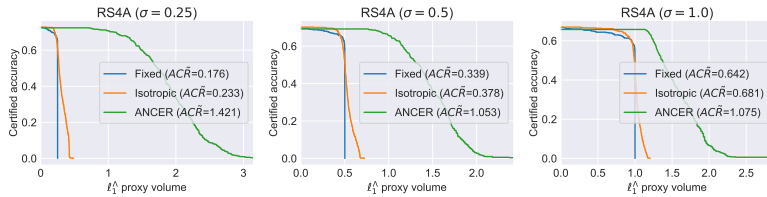


Figure 15: ImageNet certified accuracy as a function of  $\ell_1^\Lambda$  proxy radius per  $\sigma$  (used as initialization in the isotropic data-dependent case and ANCER).